Angewandte Reviews



DOI: 10.1002/anie.201207240

Nanostructures

# Emerging Strategies for the Total Synthesis of Inorganic Nanostructures

*Matthew R. Buck and Raymond E. Schaak**

**Keywords:**
colloids · hybrid particles · nanoparticles · nanostructures · synthesis design

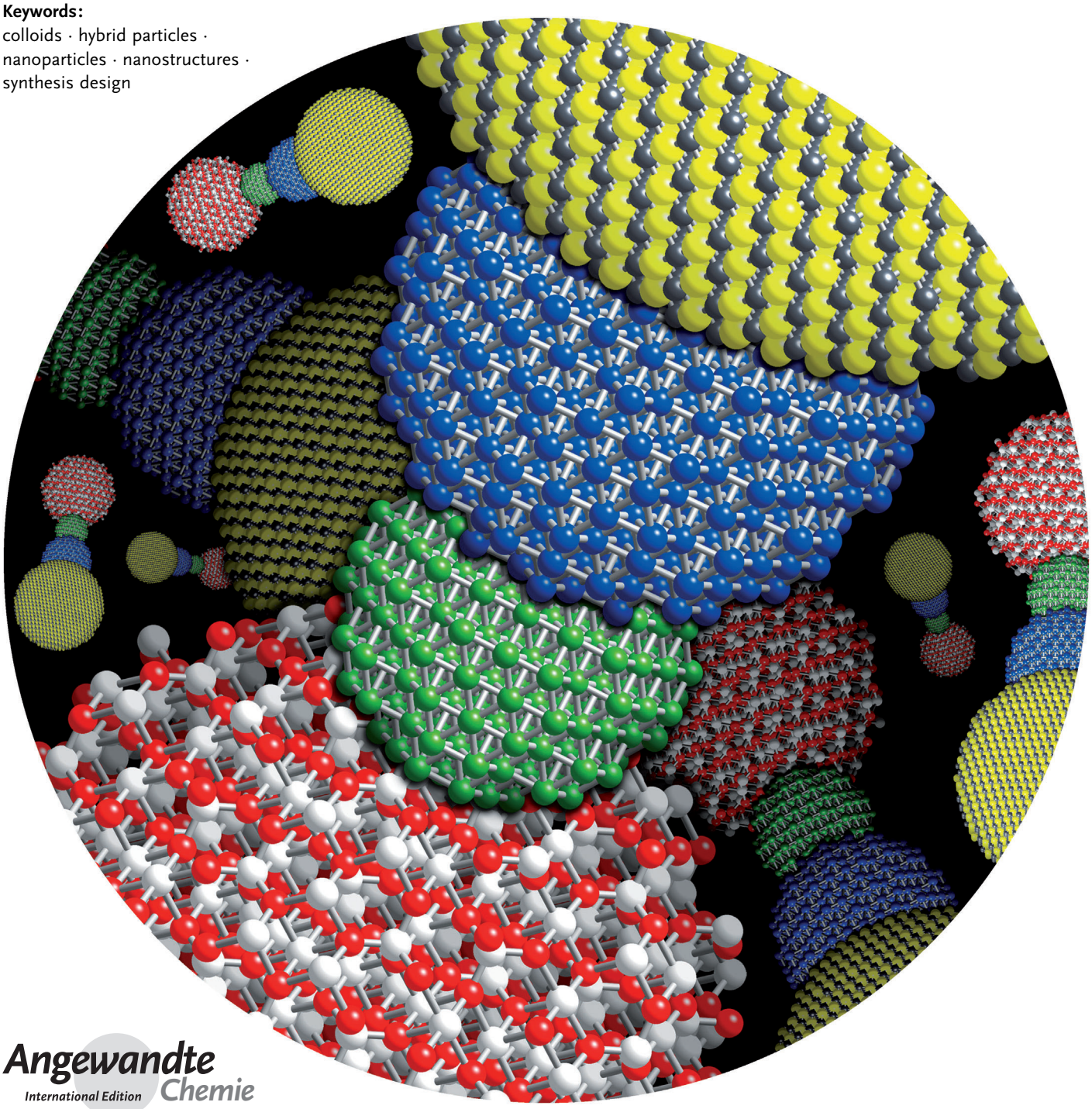

Angewandte International Edition Chemie

Angewandte International Edition Chemie

*New synthetic innovations are rapidly being developed to address the demand for complex, next-generation nanomaterials with rigorously controlled architectures and interfaces. This Review highlights key strategies for the chemical transformation and stepwise synthesis of multicomponent inorganic nanostructures, with the existing nanoscale transformations categorized into classes of reactions that are related to those used in the synthesis of organic molecules. The application of concepts used in molecular synthesis—including site-selectivity, regio- and chemoselectivity, orthogonal reactivity, coupling reactions, protection/deprotection strategies, and procedures for separation and purification—to nanoscale systems is emphasized. Collectively, the resulting synthetic concept represents an emerging model for the synthesis of complex inorganic nanostructures on the basis of the guiding principles that underpin the multistep total synthesis of complex organic molecules and natural products.*

**From the Contents**



## 1. Introduction

Sophisticated architectures of growing complexity are becoming desired for inorganic nanostructures as the applications of these materials continue to expand. Increasingly stringent boundaries are being placed on dimensionality, uniformity, and functionality, thus requiring meticulous engineering at the nanometer scale. Among the simplest nanostructures are those that contain single inorganic components, and increasingly rigorous synthetic control is needed to meet design criteria for such systems across a wide range of diverse research areas. For example, metal,[1–6] multimetal,[7,8] and metal oxide nanocrystals[9–12] bound by high-index crystal facets are desirable catalysts because they have surfaces with large densities of reactive step, ledge, and kink sites.[13,14] Thus, nanocrystals must be prepared with non-equilibrium geometries,[15–17] which is challenging because high-index surfaces are inherently energetic. Likewise, magnetic single-component nanoparticles are promising for applications such as in vivo theranostics, but the surface of each particle must be carefully engineered to support physiological stability and targeting motifs, while maintaining a high magnetic energy density for clear imaging.[18–20] Furthermore, nanoparticles with exquisite uniformity can self-assemble into highly periodic crystalline superlattices, and this has given rise to "artificial solids", which are compelling materials for electronics and energy-conversion devices.[21–25] These and many other examples emphasize the degree to which complexity and stringency have become central themes in the synthesis of nanomaterials, even for systems with only a single inorganic component.

As the trend towards complex nanoscale materials continues to expand, there is a natural progression from single-component systems to nanostructures that have multiple inorganic components. Of particular interest are multicomponent structures that are characterized by solid-state interfaces, which facilitate electronic and magnetic communication between the inorganic domains.[26–34] Interfacial phenomena of this type, such as charge transfer and spin exchange, give rise to useful properties not observed in physical mixtures of the components. Next-generation electronic devices, for example, may contain many nanoscale heterojunctions, including metal–semiconductor, semiconductor–semiconductor, and metal–metal oxide contacts. Device components such as p–n junctions, Schottky diodes, and logic gates are derived from these points of contact.[35] New and unexpected properties can also result from creating intimate contact between complementary solids. Gold nanoparticles, for example, become highly active catalysts for CO oxidation when dispersed on a variety of metal oxide supports, despite being chemically inert when isolated or supported on carbon.[36,37] Recently, tremendous effort has been invested in developing nanostructured materials that efficiently harvest, store, and utilize solar energy.[38–41] A spatially controlled arrangement of inorganic domains, which result in a prescribed sequence of heterojunctions, is the defining characteristic of many new photoactive nanomaterials.[42–44] For example, programmed arrangements of metal and semiconducting domains are designed to energetically direct the flow of separated charges, as in the recently proposed ternary Pt-$TiO_2$-$IrO_2$ heterostructure,[45] but such complex targets are still quite a synthetic challenge.

Multicomponent inorganic nanostructures are not so unlike molecules, with solid-state interfaces analogous to chemical bonds. This has been noted previously by a number of other researchers.[46,47] An electrochemical potential results in charge transfer between two solids in contact, and the magnitude of that potential determines the amount of charge transferred and its reversibility. This is akin to the electro-

[*] M. R. Buck, Prof. R. E. Schaak
Department of Chemistry and Materials Research Institute
The Pennsylvania State University
University Park, PA 16802 (USA)
E-mail: schaak@chem.psu.edu

negativity difference between two atoms that share electrons, which characterizes the polarity (or ionicity) of a bond. Even the simplest collection of atoms—a diatomic molecule such as $H_2$ or $O_2$—has properties that are vastly different from those of the isolated atoms, just as multicomponent nanostructures exhibit modulated properties relative to the constituent inorganic domains.

A complex molecule, such as an organic natural product, can be thought of as a construction of simpler molecular fragments and functional groups, with local geometries, charge distributions, and connectivities that act concertedly to impart its global function. Certain parts of a molecule may act as a scaffold, providing structural and geometrical support for the more-active functional groups. One functional group may be more active than another under certain conditions, or more directly responsible for the chemical and physical properties of the molecule. The presence of a certain element or group may also significantly influence other parts of a molecule, either through steric or inductive effects. Multicomponent inorganic nanostructures, created by piecing together simple solid-state building blocks into more complex functional architectures, can be thought of as multidomain constructs that are conceptually analogous to organic molecules. (Note that anisotropic nanocrystals with multiple distinct facets can also, by themselves, be considered to be conceptually analogous to organic molecules in cases where the unique reactivity of each facet can lead to facet-selective deposition and functionalization.) Nanoparticles that are connected by a solid-state interface often behave very differently from their isolated individual domains, with distinct properties, surface chemistries, reactivities, and affinities to transformation. Many are considered multifunctional, particularly if the different domains can play distinct roles in accomplishing multiple tasks simultaneously. Importantly, adjacent domains can have a significant impact on the properties of one another through a solid-state heterojunction. One such class of nanostructures is colloidal hybrid nanoparticles (Figure 1 a–c),[26–30] where the heterojunctions can serve as a platform for studying synergistic processes such as light-induced charge separation[48–51] and carrier dynamics,[52,53] photocatalysis,[54–56] metal–support interactions,[57–59] and exchange-biased magnetism.[60–62] One-dimensional segmented nanowires prepared by sequential, electrodeposition within a porous template are another type of nanostructure that has different materials segments linked together in a linear array (Figure 1 d).[31,63,64] These segmented nanowires have been used extensively as platforms for a wide variety of physical phenomena and applications, including nanoscale locomotion,[65–67] self-assembly,[68–70] photoconductivity,[71] biological sensing,[72–74] and catalysis.[75–77]

While there are clearly conceptual analogies between molecules and multicomponent inorganic nanostructures, there are also important differences. In a purified sample of a given compound, each molecule is precise and identical. The size and shape of a molecule, along with its arrangement of constituent atoms, are defined by the energy-minimized hybridization and directional interaction of orbitals, which gives rise to predictable bond angles and molecular geometries. Atoms and functional groups are spatially arranged, in part, as a result of the synthesis pathway. In contrast to molecules, each nanoparticle in an as-made sample has, at best, variance in its diameter of one or more atomic layers. Such variance at the "artificial atom" level guarantees that there will be size variance in any "artificial molecule," and this is especially problematic for nanoparticles that exhibit size-dependent properties. Spherical nanoparticles have surfaces that are largely equivalent regardless of spatial orientation, so attachment of a second nanoparticle to its surface typically occurs at an arbitrary site and with random "bond angles," unless the nanoparticle has clearly defined facets, each with a different surface energy and propensity for attachment or growth of a subsequent domain.[30,78,79] Molecules with multiple functional groups that are synthesized through multistep reactions are rarely accessed in near-100% yield, but chromatographic strategies for separation and purification are both readily available and routinely practiced. Despite the irregularities that are inherent in multicomponent inorganic nanostructures, strategies for separation and purification are just beginning to emerge.[80–84] Such techniques are still largely at the research and development stage, and are, therefore, of limited availability and utility. Any variance in the morphological and compositional characteristics of the hybrid nanoparticle population is typically retained in the final product.

Finally, to construct complex molecules, chemists can draw upon an extensive library of chemical reactions that permits rational modification and linking together of smaller molecular building blocks. Multistep reactions are performed in a predictive, stepwise manner, by using a synthetic approach that is guided by both mechanistic understanding and empirical insight. This contrasts sharply with the limited

*Matthew R. Buck grew up in Orange County, NY (USA) and received his BA in chemistry from The State University of New York at New Paltz in 2007. He is currently carrying out a PhD in chemistry at The Pennsylvania State University under the guidance of Prof. Raymond E. Schaak. His research focuses on the chemical synthesis of inorganic nanostructures by design, including shape-controlled metal oxide and chalcogenide nanocrystals, non-equilibrium solids, and complex hybrid nanocrystals with engineered interfaces.*

*Raymond E. Schaak grew up in Palmyra, PA (USA) and received a BS in chemistry from Lebanon Valley College in 1998. He earned his PhD in chemistry in 2001, working with Prof. Thomas Mallouk at Penn State University. After postdoctoral research with Prof. Robert Cava at Princeton University, he became an assistant professor of chemistry at Texas A&M University in 2003. He moved to Penn State University in 2007, where he is currently a professor of chemistry. His research focuses on the development of new approaches for the synthesis of inorganic solids and nanostructures.*

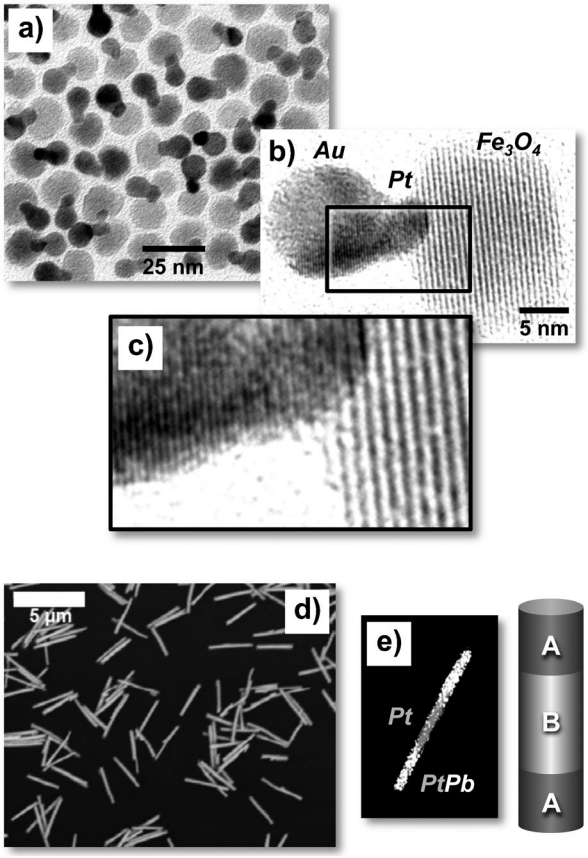


***Figure 1.*** a–c) TEM images, at three different magnifications, of colloidal Au-Pt-$Fe_3O_4$ heterotrimers synthesized by the addition of an $Fe_3O_4$ domain to Pt nanoparticles to form Pt-$Fe_3O_4$ heterodimers through heterogeneous seeded growth, followed by the addition of Au to the Pt domain of the Pt-$Fe_3O_4$ heterodimers. d,e) SEM images and schematic representation of segmented PtPb-Pt-PtPb nanowires synthesized by chemical conversion of the ends of Pt nanowires confined within an anodic aluminum oxide membrane. Panels (a–c) reprinted from Ref. [174] with permission (Copyright 2011, Macmillan Publishers Limited) and panels (d,e) reprinted from Ref. [180] with permission (Copyright 2008, American Chemical Society).

reaction repertoire and mechanistic understanding available to chemists constructing multicomponent inorganic nanostructures, and sequential multistep reactions are rare. A "total synthesis" approach that is conceptually analogous to that taken by chemists to synthesize complex molecules and natural products would greatly expand our capabilities for the deterministic and by-design synthesis of complex multicomponent inorganic nanostructures with predefined morphological features and, accordingly, designer properties and functions. Such a synthetic approach would require both an expanded reaction library and mechanistic insights.

In the sections that follow, we begin by highlighting some of the most important concepts that underpin the chemical synthesis of organic molecules. We then discuss the currently available reactions for nanoparticles, emphasizing a classification scheme for these nanoparticle transformations that explicitly links them to molecular reactions. Indeed, if one thinks about individual nanoparticles as conceptually analogous to molecular functional groups, then reactions that modify nanoparticles can be thought of as conceptually analogous to textbook organic reactions. We then move to the application of such reactions to multicomponent inorganic nanostructures, which parallels those transformations that target a specific functional group or moiety on a larger molecule that contains multiple reactive sites. Moving beyond reactions, we then detail some of the key synthetic strategies that underpin the construction of both complex molecules and complex multicomponent inorganic nanostructures, such as site-specific reactivity, orthogonal reactivity, and protection/deprotection. With this framework, we then discuss how a "total synthesis" approach could be used to construct high-order hybrid inorganic nanostructures through sequential multistep reactions. Finally, we discuss the need for purification, separation, and detailed reporting about yield. These procedures and the information that they provide are ubiquitous in organic synthesis but are not mainstream for inorganic nanostructures, despite the possibilities and applications that emerge as a direct result of such postsynthesis work-up and analysis.

## 2. The "Working Principles" of Molecular Total Synthesis

Many important details go into successfully implementing the total synthesis strategies that are used to construct large, complex molecules, and these are covered extensively in numerous textbooks and articles.[85–87] However, stepping back from the details—which are clearly different from those used in the synthesis and chemical transformation of nanoparticles—there are a number of concepts, or "working principles," that underpin such efforts, and are important to consider for possible applicability to nanoparticle systems (Figure 2). First, it is usually desirable to start with reasonably simple molecular fragments that can be easily made or acquired and that structurally mimic a part of the target molecule (Figure 2a).[88,89] Such molecular building blocks will typically contain reactive functional groups at specific locations, which permit desired chemical modifications to be carried out in a systematic and stepwise manner. The types of chemical reactions used to modify and build outward from these molecular precursors are both extensive and diverse, and new reactions with expanded capabilities continue to be frequently reported (Figure 2b).[90] Many of these reactions are named after the chemists who first reported them and are often considered as "textbook reactions" because of their widespread use. A non-exhaustive list of classes of reactions includes oxidation, reduction, addition, substitution, elimination, condensation, cleavage, metathesis, coupling, cyclization, cycloaddition, group transfer, and ring opening.

Guiding principles exist for carrying out transformations on molecules where multiple reactive functional groups may be present or where multiple sites may facilitate a particular reaction (Figure 2c). An understanding of the principles governing selectivity allows chemists to direct reactions to occur at specific locations on a molecule, thus leading to a targeted product.[91–93] Chemoselective reactions, for example, target one functional group when others are also

  

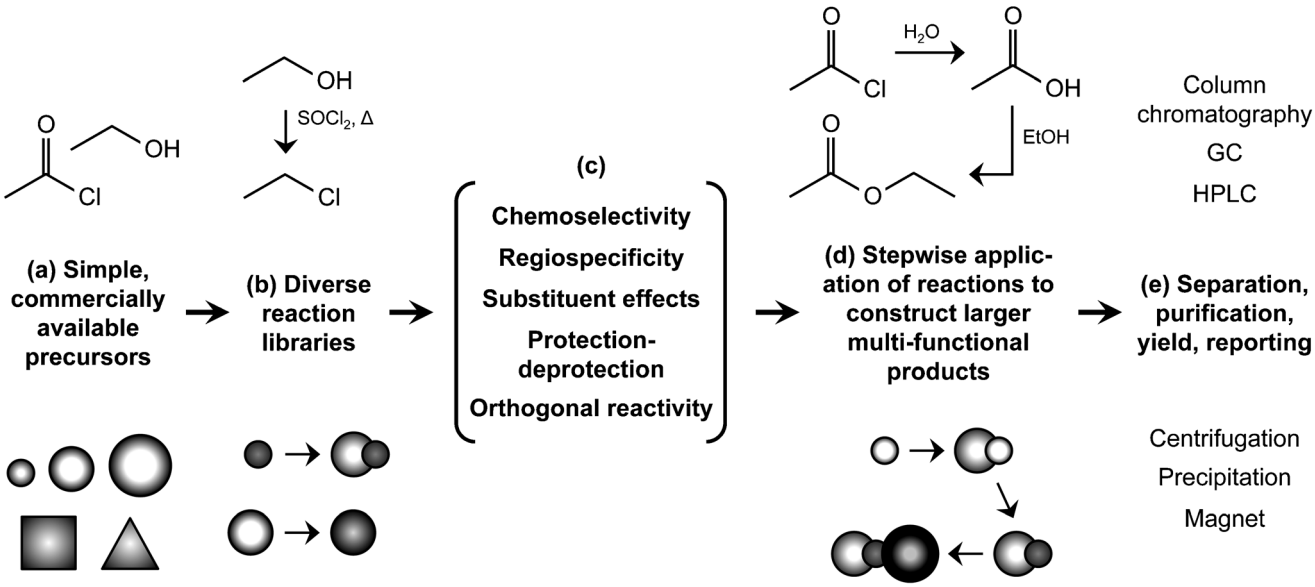


***Figure 2.*** A multistep synthetic concept for molecules (top) and nanoparticles (bottom), along with chemical structures and graphical examples.

present—as exemplified by the borohydride-mediated reduction of ketones and aldehydes to alcohols. This reduction can be carried out in the presence of a carboxylic acid or an ester, which remain unaffected by the borohydride ion. Another working principle is regioselectivity, which preferentially generates products that have a particular connectivity when other isomers may be possible, as is the case with electrophilic aromatic substitution reactions. Here, electron-donating and -withdrawing groups have a powerful influence over whether substitution occurs at the *ortho*, *meta*, or *para* positions of a benzene ring. When selectivity is required but is not possible for a particular set of functional groups and available reagents, undesired reaction pathways can sometimes be shut down by installing protecting groups on one or more of the reactive moieties, while carrying out subsequent reactions only on those that remain exposed.[94] After carrying out such a reaction, the protecting group can be removed to re-expose the other functional group(s). Protection/deprotection strategies are powerful for targeting desired reaction sites and achieving selectivity in complex or multifunctional systems. Collectively, such strategies serve to facilitate orthogonal reactivity, where one functional group on a multifunctional molecule reacts in a desired way with a particular reagent under a given set of conditions while other functional groups on the same molecule do not.

Total synthesis consists of the purposeful, stepwise execution of available chemical reactions, implemented in a way that permits precise targeting of the desired functional groups at specific locations on a molecule (Figure 2d).[85,87] Indeed, the power of total synthesis is not simply the reactions and their mechanisms (although this is clearly important), but rather the ability to integrate multiple reactions in a predictable and sequential manner to allow the rational design and deterministic synthesis of an arbitrary molecule with predefined geometries, linkages, functional groups, and spatial organization. Another important practical consequence of this approach is the availability of multiple reactions, each with distinct capabilities and unique sets of advantages and disadvantages, which can lead to the same product. For example, there are a variety of approaches that can result in the installation of an OH group on a molecule. Considerations such as the reaction conditions, the stability and reactivity of the candidate reagents, the possible side reactions and conceivable products associated with each approach, and the types and locations of other (possibly competing) functional groups, along with empirical guidelines, dictate when one of the available reactions is preferable over another. Finally, another practical consequence of multistep pathways to complex molecules is the decreasing yield with each additional reaction. In one sense, this is not a problem, because separation and purification tools are both widely available and routinely utilized (Figure 2e). However, at the same time, yields are maximized when reactions go as far towards completion as possible and when reactions are carried out as selectively and as efficiently as possible, so that by-products and undesired isomers are avoided and the number of steps in the synthesis is minimized.[95–97] Indeed, one of the key metrics of a successful multistep synthesis is the product yield, and data to demonstrate purity of the final product (NMR, IR, and UV/Vis spectroscopy, GC-MS, melting point, etc.) are both readily achievable and demanded by the scientific community. These "working principles" of molecular total synthesis are also applicable to the construction of multicomponent nanostructures, although the details of how the concepts are implemented are very different (Figure 2). The sections that follow will emphasize both the similarities and differences.

## 3. Nanoparticle Reaction Libraries

When planning the synthesis of a complex molecular target, chemists identify simple building blocks that can be adjoined, split apart, or modified by relying on libraries of

well-understood chemical reactions. These transformations are often classified according to the type of synthon. For example, it is known that acyl chlorides react with alcohols to produce esters, undergo hydrolysis to form carboxylic acids, react with amines to generate amides, and react with carboxylic acids to make acid anhydrides. Alternatively, generalized types of reactions can be grouped together, including nucleophilic substitution, elimination, addition, electrophilic aromatic substitution, and condensation reactions. During the past decade, a large body of research has been dedicated to generating libraries of chemical transformations for nanoparticles, which are the building blocks of multicomponent nanostructures. This approach demonstrates that a preformed nanoparticle can be utilized as a synthon to generate a more-complex derivative, in a manner that is similar to functional group transformation in organic synthesis.[98] Nanoparticle transformations, similar to molecular reactions, can be classified either by synthon type (metallic nanoparticles, ionic nanocrystals, etc.; see Figure 3) or by reaction type (e.g. oxidation, coupling, etc.; see Figure 4). Below, we will outline the most important types of nanoparticle reactions, including oxidative diffusion, reductive diffusion, metal diffusion, cation exchange, anion exchange, heterogeneous seeded growth (addition), dissolution (elimination), galvanic replacement, and coupling reactions. Detailed reviews of nanoparticle transformation reactions have been published,[99,100] and are not duplicated here; important and more recent highlights are included below.

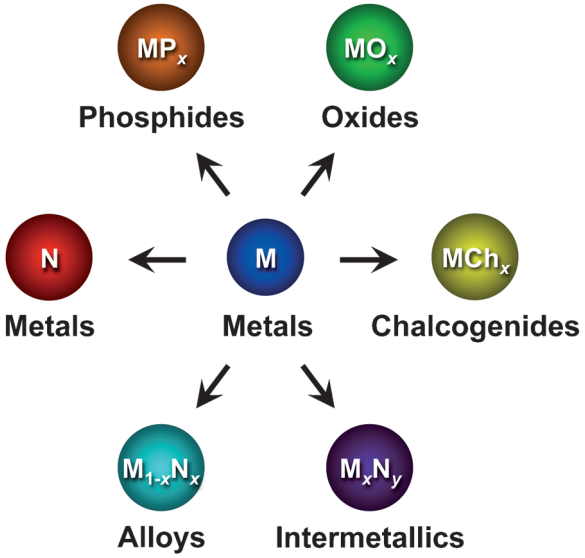


***Figure 3.*** Classes of compounds that are commonly accessible by solution-phase chemical transformation reactions of metal nanoparticle synthons.

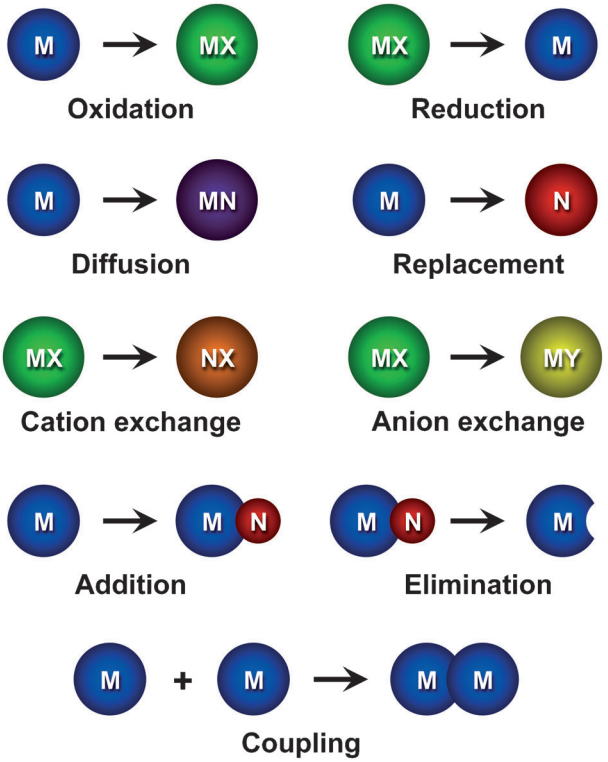


***Figure 4.*** Categories of solution-phase chemical transformation reactions that are commonly used to convert one type of nanoparticle into another.

Single-element metal nanoparticles are straightforward to prepare for many systems, and can be subsequently reacted in a wide variety of ways. Oxidative diffusion reactions can be performed on metal nanoparticles to synthesize the corresponding metal oxides, chalcogenides, phosphides, and nitrides. Cobalt nanoparticles, for example, oxidize spontaneously in the presence of oxygen to form CoO,[101] react readily with molecular sources of sulfur and selenium to form a variety of $Co_xS_y$ and $Co_xSe_y$ phases,[101,102] and transform into CoP or $Co_2P$ in the presence of thermally decomposed trioctylphosphine (TOP).[103,104] Similarly, when cationic metal precursors are reduced in the presence of metal nanoparticles, metallurgical diffusion reactions can transform metal nanoparticles into alloy and intermetallic phases.[105] The rate of diffusion is significantly enhanced when the elemental product of metal salt reduction has a relatively low melting point, such as Pb, Sn, Bi, or In. Moreover, the rate-limiting step of solid–solid diffusion in bulk metallurgical processes is bypassed in reactions involving small metal nanoparticles, because the reduced dimensions result in short diffusion distances. Intermetallic and alloy nanoparticles of FePt, $FePt_3$, CoPt, PtPb, PtSn, PtBi, PtSb, $Cu_3Pt$, and other derivatives, for example, can all be prepared in solution by using Pt nanoparticles as a reactive precursor.[105–107]

Diffusion reactions involving the oxidation of metal nanoparticles are far more common than transformations involving the reduction of ionic nanocrystals, but there are a few important examples. The reduction of metal oxide particles is a common method to prepare catalysts with supported metal nanoparticles, and this is usually accomplished by thermal treatment in hydrogen or by a chemical reagent such as formaldehyde or hydrazine.[108] It was also shown recently that TOP, when heated in the presence of binary metal chalcogenide nanoparticles, induces partial reduction to selectively extract sulfur or selenium.[109] The

  

as-made particles were typically chalcogenide-rich phases, such as $SnSe_2$, $FeS_2$, $NiSe_2$, and $CoSe_2$, which conveniently convert into the most metal-rich phases (SnSe, FeS, $Ni_3Se_2$, and $Co_9Se_8$) on heating in TOP at temperatures ranging from 65° to 270 °C.

Ionic nanocrystals, including the so-called quantum dots, are susceptible to useful cation exchange reactions (Figure 5), which are typically driven by a higher solubility of the preformed nanoparticles in the surrounding medium than the target compound.[110–119] For example, CdS and CdSe nanoparticles react rapidly at room temperature with either $Cu^+$ or $Ag^+$ ions in methanol/toluene mixtures to form $Ag_2S$, $Ag_2Se$, $Cu_2S$, or $Cu_2Se$.[110,112,114] Partial cation exchange has also been realized, thereby giving rise to segmented CdS-$Ag_2S$[112] and CdS-$Cu_2S$ nanorods[115] starting from CdS nanorods (Figure 5a,b). Significantly, many of these transformations proceed with morphological retention of the substrate particle because of conservation of the anion sublattice during exchange,[116] and are reversible based on the concentration and solvation energies of incoming and outgoing ions. Recently, multiple cation exchange reactions have been carried out sequentially using CdSe nanocrystals as a starting material, which were first treated with $Cu^+$ ions to make $Cu_{2-x}Se$ ($0 \le x < 1$) and then treated with $Zn^{2+}$ ions to generate ZnSe (Figure 5c–e).[117] In this case, the transformation from the more-stable $Cu_{2-x}Se$ to the lower lattice energy ZnSe was made favorable by high temperatures (250 °C) and strong interactions between the solution-phase ligands and $Cu^+$ ions that were extracted from the lattice. Another important consequence of the conservation of the anion sublattice is the transfer of crystal-structure information to the product nanocrystals, which has enabled access to non-equilibrium solids that are otherwise difficult to prepare. In the previous example, hexagonal (hcp) wurtzite-type CdSe nanocrystals converted into a metastable hcp phase of $Cu_{2-x}Se$ (the stable hcp phase is 1:1 CuSe), and again to metastable hcp wurtzite-type ZnSe (Figure 5f). ZnSe typically crystallizes as the cubic (fcc) sphalerite phase.

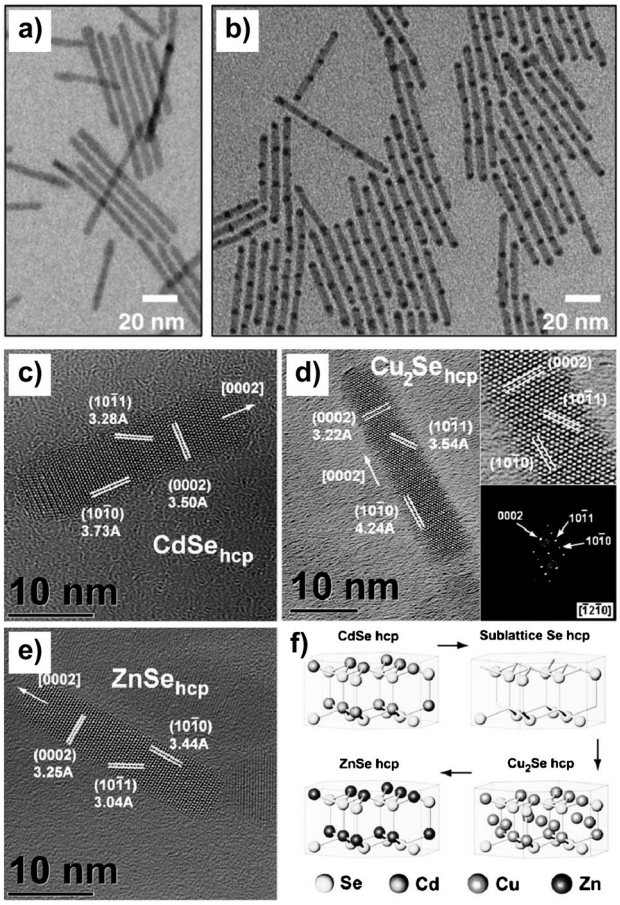


***Figure 5.*** Representative examples of nanoscale cation exchange reactions: TEM images of a) CdS nanorod precursors and b) CdS-$Ag_2S$ superlattice nanorods after partial ion exchange of the CdS nanorods with $Ag^+$, and HRTEM images of c) wurtzite-type CdSe nanorods, d) wurtzite-type $Cu_2Se$ nanorods after ion exchange of the CdSe nanorods in (c) with $Cu^+$, and e) wurtzite-type ZnSe nanorods after ion exchange of the $Cu_2Se$ nanorods in (d) with $Zn^{2+}$. The conserved anion lattice, which leads to retention of the wurtzite structure type, is shown in (f). Panels (a,b) reprinted from Ref. [112] with permission (Copyright 2007, American Association for the Advancement of Science) and panels (c–f) reprinted from Ref. [117] with permission (Copyright 2011, American Chemical Society).

Anion exchange is also a powerful technique for reacting ionic nanocrystals (Figure 6). Wurtzite-type ZnO nanoparticles, for example, are intermediates in the reaction between $ZnCl_2$ and thio- or selenourea in polyol solvents containing hydroxide ions.[120] The transient ZnO particles act as a structural template for the formation of metastable wurtzite-type ZnS and ZnSe (Figure 6b), again highlighting the conserved sublattice crystal structure during the transformation (Figure 6a). Building upon this observation, single-crystal wurtzite-ZnS shells with a hollow interior were generated by treating colloidal ZnO nanocrystals with hexamethyldisilathiane (Figure 6c,d).[121] A void was formed in the core of each ZnS particle as a result of the nanoscale Kirkendall effect, whereby outward $O^{2-}$ diffusion was faster than inward $S^{2-}$ diffusion, and the hexagonal pyramidal shape of the ZnO nanocrystals was conserved in the process. More recently, wurtzite-type CdS was treated with tri-*n*-octylphosphine telluride (TOP-Te) to form zinc blende CdTe nanocrystals.[122] If this reaction was allowed to go only partially to completion, anisotropically phase-segregated CdS-CdTe heterodimers were isolated, as a consequence of strain induced by the different crystal structures at the CdS–CdTe interface.

Heterogeneous seeded-growth reactions have been used to generate libraries of multicomponent colloidal hybrid nanostructures, including an extensive variety of core–shell and a smaller (but growing) number of nonconcentric heterooligomer-type geometries (Figure 7). This synthetic innovation is relatively new, and is a result of two primary motivations: 1) The ability to introduce additional functionality into an already functional unit, thereby giving rise to multifunctional nanostructures with useful property combinations that may be able to accomplish multiple tasks simultaneously and 2) the desire to study how inorganic domains synergistically communicate when adjoined by a solid-state interface. Conceptually, the introduction of a new functionality to a preexisting unit is analogous to an

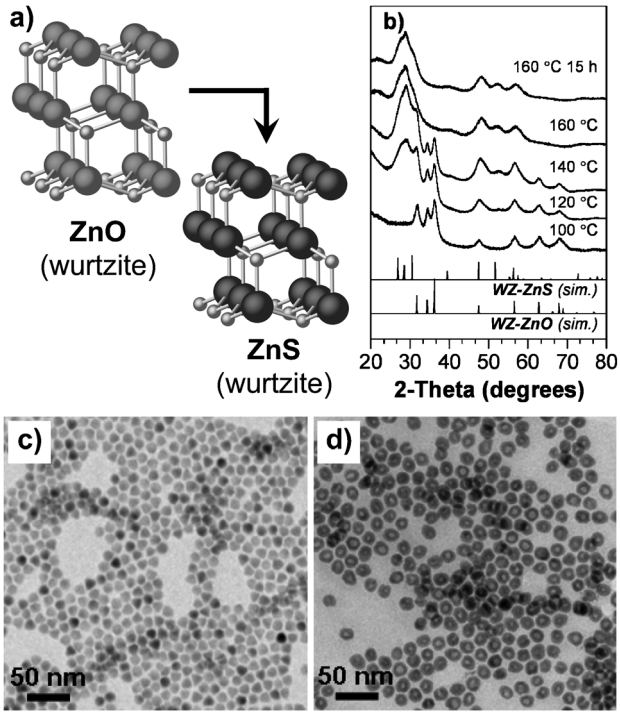


***Figure 6.*** Representative examples of nanoscale anion-exchange reactions: a) Powder XRD data characterizing the transformation of wurtzite-type ZnO into wurtzite-type ZnS, b) crystal structures of the ZnO precursor and ZnS product, highlighting the retained cation sublattice, and TEM images of c) ZnO nanoparticles and d) hollow single-crystal ZnS nanoparticles synthesized by treating the ZnO nanoparticles in (c) with hexamethyldisilathiane in trioctylphosphine. Panels (a,b) reprinted from Ref. [120] with permission (Copyright 2009, American Chemical Society) and panels (c,d) reprinted from Ref. [121] with permission (Copyright 2009, American Chemical Society).

addition reaction in organic synthesis, such as the epoxidation of olefins. The study of heterogeneous seeded growth has already given rise to numerous metal–metal, metal–metal oxide, metal–semiconductor, metal oxide–semiconductor, and semiconductor–semiconductor hybrid nanostructures with a variety of two-component architectures, and the library is growing rapidly. These results are summarized in a number of recent review articles.[26–30]

As the name implies, seeded-growth "additions" require a second inorganic domain to grow directly from the surface of a preformed nanoparticle seed, which is usually accomplished by selecting reaction conditions that suppress homogeneous nucleation of isolated nanoparticles. Conditions that promote heterogeneous nucleation include much lower concentrations of molecular precursors and lower temperatures than are normally required to nucleate single-component nanoparticles. The final morphology of colloidal hybrid nanostructures (core–shell, anisotropic, multidomain, etc.), however, is influenced by many variables. In many cases, these variables are elucidated largely on the basis of empirical observations and they can be system-dependent, including lattice matching, solvent polarity, heating rate, seed-to-precursor ratio, surfactant concentration, and the availability of reactive crystal facets on the seeds. Despite the lack of materials-general observations regarding what governs the morphology of colloidal hybrid nanostructures, sophisticated hypotheses are continually being developed, substantiated by in-depth characterization of solid–solid interfaces and mechanistic insights.[123–125] For example, Cao and co-workers carried out extensive high-resolution transmission electron microscopy (HRTEM) studies on FePt-$In_2O_3$ heterodimer nanoparticles and revealed that FePt(110) and $In_2O_3$(222) junctions as well as FePt(200) and $In_2O_3$(440) junctions were both present in their samples, with the population heavily weighted toward the former. This was surprising, because the lattice pair FePt(200)/$In_2O_3$(440) was more closely matched than the FePt(110)/$In_2O_3$(222) pair, which suggested that the coordination environment of atoms at the FePt–$In_2O_3$ interface and bond strengths play a more important role than minimization of lattice mismatch.[124]

An analogue of organic elimination reactions, rather than addition, is also useful in the synthesis of nanostructures, and can be considered as the simple dissolution or etching of an inorganic solid. There have been many examples of both in situ and postsynthetic modification of metal nanoparticles (i.e. Au, Ag, Pt, Pd) by using crystallographically selective wet etchants, which have resulted in unconventional, non-equi-

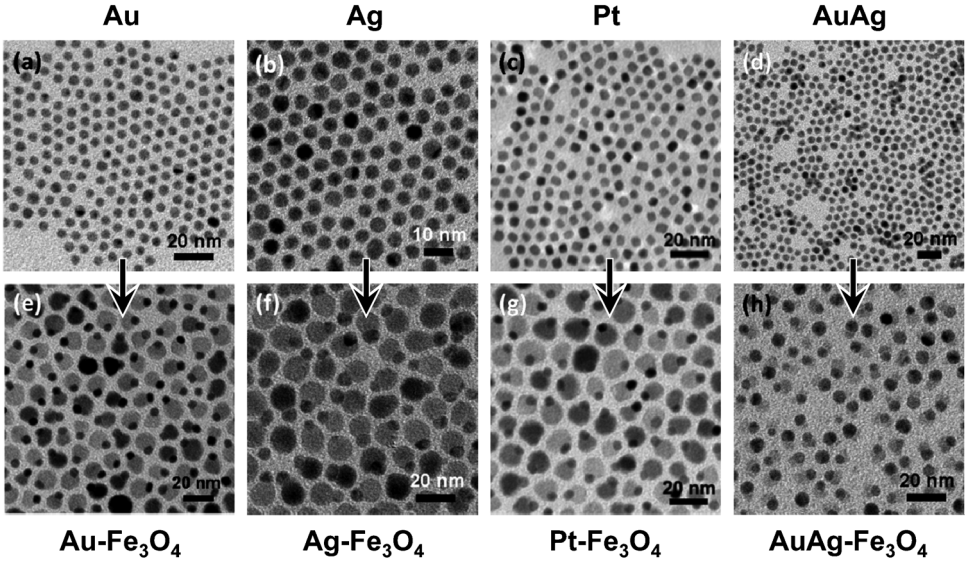


***Figure 7.*** Representative examples of nanoscale addition reactions: TEM images of a) Au, b) Ag, c) Pt, and d) AuAg nanoparticle seeds, and e) Au-$Fe_3O_4$, f) Ag-$Fe_3O_4$, g) Pt-$Fe_3O4$, and h) AuAg-$Fe_3O_4$ hybrid nanoparticle products formed by heterogeneous seeded growth of $Fe_3O_4$. Reprinted from Ref. [59] with permission (Copyright 2010, American Chemical Society).

  

librium morphologies.[126–129] Metal nanoparticles can also be sacrificially oxidized by metal cations having a higher reduction potential, and thereby galvanically replaced to create new metal and alloyed nanostructures that often have a hollow interior.[130–133] For example, Ag nanocrystals with a wide variety of shapes can be prepared readily and subsequently treated with $AuCl_4^-$ ions to make hollow Au and AuAg alloy nanostructures.

Preformed nanoparticles can also be controllably positioned or grouped into stoichiometrically controlled clusters by using "coupling" processes. This topic has been reviewed.[46,47,134] Coupling reactions allow nanoparticles to be spatially and geometrically arranged in proximity to one another to examine how the properties of the ensemble depend on its dimensionality and differ from those of the isolated particles. This is particularly interesting for coupling plasmonically active (i.e. Au, Ag, Cu) nanoparticles, because the hybridization of the surface plasmon resonance is strongly dependent on interparticle distance, which has important implications for monitoring biological processes by microscopy and spectroscopy.[134] The coupling of inorganic nanoparticles is often facilitated by molecular interactions with a high degree of chemical recognition, such as DNA base pairing, antibody–receptor binding, predictable Lewis acid/base pairing (such as Au/thiol), and surface-ligand polymerization. In some cases, coupling is achieved by oriented attachment, where two or more nanoparticles come together with crystallographic alignment to form a solid–solid interface across a particular facet. This process eliminates a significant fraction of undercoordinated surface atoms, and is therefore driven by minimization of the surface energy.[135] Alternatively, groupings of nanoparticles can also be encapsulated within inorganic glass and/or polymer matrices or, for larger colloids, can form through controlled dewetting or liquid-phase encapsulation techniques. A variety of architectures have been achieved through controlled coupling, including dimers, trimers, tetramers, linear chains, branched chains, and other network-type geometries. Another strategy for nanoparticle coupling involves the thermally driven interdiffusion of two or more preexisting domains. When applied to multidomain nanostructures, which will be discussed in Section 4.2, high-order oligomers and complex solid-state networks can be formed without the need for molecular or biological linkers.

## 4. Reactions for Multicomponent Inorganic Nanostructures

The previous section described many chemical conversion reactions that have been used to transform single-domain nanoparticles, and their similarity to organic transformations. Far fewer reports exist, however, of the use of analogous reactions to modify inorganic nanostructures that have multiple domains. When the substrate to be modified possesses more than one component, a number of interesting questions arise: Is the given reaction selective for one of the components, or will multiple domains react under these conditions? Can reaction conditions be found that promote preferential conversion of one component? Does the component to be modified react differently in the heterostructure than it does when isolated? How is the mechanical and structural integrity of the heterojunction affected by the reaction: Is it robust or weak? In many ways, these questions and the associated challenges are similar to those that organic chemists encounter when planning the synthesis of a complex molecule. Below, we highlight the synthetic concepts that are unique to multicomponent structures, including orthogonal reactivity, site-selective transformations, coupling reactions, and protection/deprotection strategies, along with the reactions that have been demonstrated to facilitate this in nanoscale systems.

### 4.1. Orthogonal Reactivity and Site-Selective Transformations

Some of the most powerful tools for transforming multicomponent nanostructures are those reactions that proceed with site selectivity, which enables the controlled positioning of a specific functionality within a multifunctional object. Simply put, site-selective reactions either fully or partially transform one domain in a multidomain nanostructure while leaving others unmodified. Site-selective transformations are enabled when the reactivities of different components within a heterostructure are said to be *orthogonal* to one another, that is, when one (or part of one) component is susceptible to transformation under a particular set of conditions while the other components do not react. Site selectivity is in some cases predictable: for example, standard reduction potentials ($E^o$, $M^{n+}/M$) dictate that certain components within a heterostructure will react readily with an oxidant (i.e. Fe, Co, Ni, Cu) while others will not (i.e. Au, Pt, $Fe_2O_3$) over a wide range of relevant reaction conditions. Orthogonal reactivity is not always intuitive, however, and those transformations that proceed site selectively are fertile ground for in-depth mechanistic studies and development.

Oxidative, reductive, and metallurgical diffusion-mediated reactions are useful for modifying single-component nanoparticles, but application of these types of transformations to multidomain nanostructures is comparatively rare. In many of these cases, however, diffusion reactions can site-selectively transform a targeted component without significantly altering the heterostructured morphology. To demonstrate this principle, Leonard et al. investigated some metallurgical diffusion reactions of physical mixtures of metal nanoparticles (Ni, Cu, Rh, Pd, Ag, Pt, Au, and Sn) with metal salts under reducing conditions at several temperatures, and observed a number of orthogonal relationships.[107] Although different nanoparticles reacted with the same metal salt solution, they did so at significantly different temperatures, thereby providing a basis for reacting a targeted component in the presence of several reactive species. For example, many metal nanoparticles reacted with Sn to form binary intermetallic compounds, but AuSn formed near room temperature, $Ni_3Sn_4$ formed at 100 °C, $Ag_4Sn$ formed at 175 °C, and $PdSn_2$ and PtSn formed at 200 °C. These observations, along with the knowledge that some combinations of metal nanoparticles and metal salts did not react, allowed one-pot two-component

  

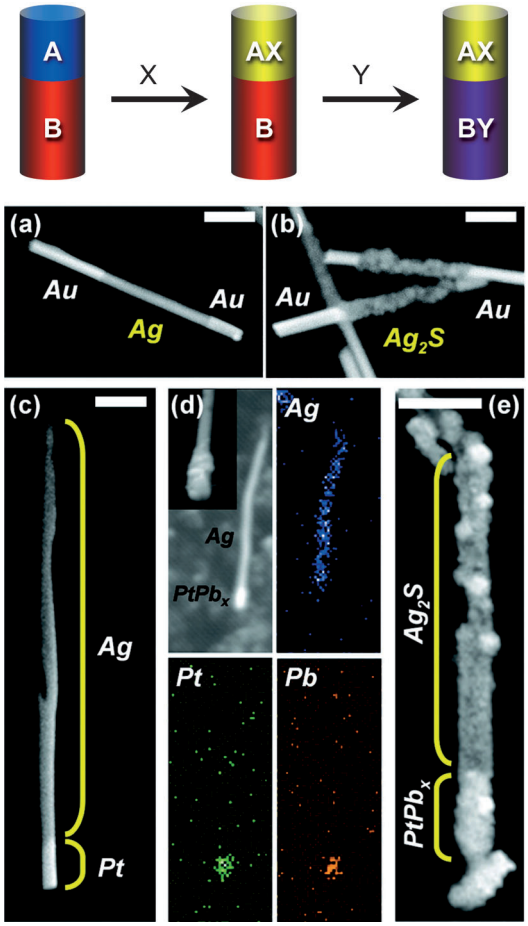


***Figure 8.*** Top: Schematic representation highlighting orthogonal reactivity in striped metal nanowire systems: Reagent X reacts with A to form AX, but does not react with B; reagent Y reacts with B to form BY, but does not react with AX. SEM images of a) an Au-Ag-Au striped metal nanowire and b) Au-$Ag_2S$-Au nanowires formed after reacting with sulfur. SEM images of c) an Ag-Pt striped metal nanowire, d) an Ag-$PtPb_x$ striped nanowire after reacting the Ag-Pt nanowire with Pb (element maps show incorporation of Pb into the Pt segment, but not the Ag segment), and e) an $Ag_2S$-$PtPb_x$ striped nanowire after treating the Ag-$PtPb_x$ nanowire with sulfur. Scale bars: 1 μm. Panels (a–e) reprinted from Ref. [107] with permission (Copyright 2009, American Chemical Society).

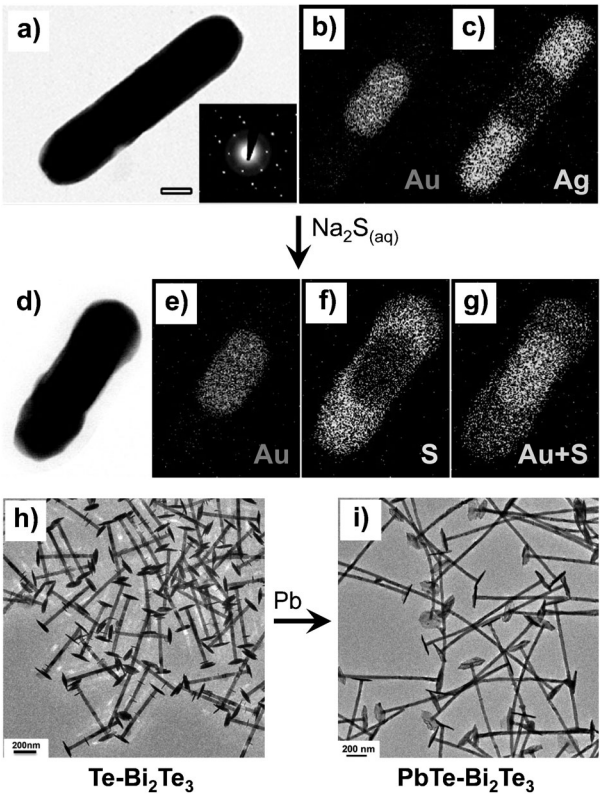


***Figure 9.*** a) TEM image (scale bar: 50 nm), electron diffraction pattern, and b) Au and c) Ag elemental mapping data for a colloidal Ag-Au-Ag striped nanorod. d) TEM image and elemental mapping data of striped $Ag_2S$-Au-$Ag_2S$ nanorods for e) Au, f) S, and g) Au + S, The nanorods were formed after treating the Ag-Au-Ag nanorods with aqueous $Na_2S$. TEM images of h) $Bi_2Te_3$ nanowires with Te tips and i) $Bi_2Te_3$ nanowires with PbTe tips after treating the $Bi_2Te_3$-Te nanowires with Pb. Panels (a–g) reprinted from Ref. [136] with permission (Copyright 2008, American Chemical Society) and panels (h,i) reprinted from Ref. [140] with permission (Copyright 2012, American Chemical Society).

orthogonal reactivity to be demonstrated in several systems. A mixture of Ag and Ni nanoparticles, for example, was treated with $SbCl_3$ at 100 °C to form intermetallic NiSb, leaving the Ag unreacted, and the mixture of Ag and NiSb nanoparticles was then treated with $SnCl_2$ at 175 °C to form a mixture of $Ag_4Sn$ and unreacted NiSb nanoparticles.

These and other derived orthogonal relationships were then applied to the controlled modification of electrochemically deposited segmented nanowires, which resulted in the synthesis of various linearly patterned, multielement, multidomain nanowires (Figure 8). For example, three-domain Au-Ag-Au striped nanowires reacted with sulfur to generate Au-$Ag_2S$-Au wires, wherein sulfur reacted selectively with the Ag domains and not with Au (Figure 8a,b).[107] Similarly, Seo et al. have shown that colloidally grown Ag-Au-Ag nanorods dispersed homogeneously in water (Figure 9a–c) can be converted into $Ag_2S$-Au-$Ag_2S$ by treatment with $Na_2S$ (Figure 9d–g).[136] Electrodeposited nanowires with Ag and Pt segments reacted under reducing conditions with Pb-$(CH_3COO)_2$ to form Ag-$PtPb_x$ nanowires ($PtPb_x$ is a mixture of PtPb and $Pt_4Pb$ phases), which were reacted subsequently with sulfur to generate segmented $Ag_2S$-$PtPb_x$ nanowires (Figure 8c–e).[107] This two-step synthesis relied on the fact that $Pb^0$ reacts readily with Pt over a wide range of temperatures, but not with Ag, and that $PtPb_x$ is resistant to sulfidation, thus allowing sequential, site-selective conversion of each domain. Solution-phase diffusion reactions represent an alternative to the ostensibly tedious, system-specific optimization required for electrochemical co-deposition of such multielement and nonconducting segments. Other spatially organized, multidomain nanostructures, such as lithographically patterned surfaces and wires, are also viable substrates for stepwise modification through diffusion reactions.[107]

Unlike template-grown striped nanowires and patterned surfaces, colloidal hybrid nanoparticles can be dispersed homogeneously in a variety of solutions, and would seem to

  

be ideal substrates for chemical modification by using site-selective diffusion reactions. There are, however, surprisingly few examples. Heterodimers of Pt-$Fe_3O_4$ are typically prepared by thermally decomposing [$Fe(CO)_5$] in the presence of Pt nanoparticle seeds, which forms intermediate Pt-Fe heterodimers that require the Fe domain to be subsequently treated with $O_2$. Similarly, a conformal shell of Fe has been deposited around Au seeds, and subsequently oxidized by bubbling air through the product mixture to obtain Au/$Fe_3O_4$ core/hollow-shell (also called yolk–shell) nanoparticles.[137] Other yolk–shell structures, which are interesting platforms for biological imaging and drug delivery, include Pt/CoO,[101] FePt/$Fe_3O_4$,[138] and FePt/$CoS_2$,[139] which were prepared by treating the corresponding Pt/Co, FePt/Fe, and FePt/Co core–shell nanoparticles with either $O_2$ or sulfur. The Kirkendall effect was responsible for the formation of voids between the core and the shell. Very recently, Te-$Bi_2Te_3$ hybrid nanoparticles with a barbell-like morphology have been synthesized for thermoelectric studies, where $Bi_2Te_3$ rods are flanked by plate-like tips of Te (Figure 9 h). The Te termini were then reacted selectively with $Pb^{2+}$ under reducing conditions to form PbTe-$Bi_2Te_3$ hybrid particles with the same morphology (Figure 9 i), and the authors speculate that Pb could possibly be replaced with a variety of other metals that react with Te, such as Ag, Sn, and Sb.[140]

Orthogonal reactivity in cation-exchange reactions has been observed for several ionic nanocrystal systems and utilized to synthesize multidomain nanostructures. Information regarding the synthesis of dimensionally controlled cadmium chalcogenide nanocrystals is abundant, thus making CdX (X = S, Se, Te) quantum dots, rods, and branched structures ideal starting points for studying cation-exchange reactions. Although $Cd^{2+}$ ions are extracted and readily replaced with soft metal cations ($Ag^+$, $Cu^+$, $Pd^{2+}$, $Pt^{2+}$) in polar solvent mixtures (methanol/toluene, aqueous/organic),[110,113,119] conditions that allow other metal cations ($Pb^{2+}$, $Zn^{2+}$) to exchange with $Cd^{2+}$ are more difficult to find. To circumvent this challenge, Luther et al. devised a two-step synthesis of PbS nanocrystals that relied on the formation of trialkylphosphine–copper(I) and—silver(I) complexes to extract either $Cu^+$ or $Ag^+$ efficiently from their respective lattices in the presence of $Pb^{2+}$ ions.[114] In the previous section we described a similar, sequential cation-exchange-enabled synthesis of ZnSe nanocrystals, by using CdSe as a template and proceeding through a $Cu_2Se$ intermediate phase.[117] In other words, the reactivities of CdX and $Cu_2X$ (or $Ag_2X$), with cations such as $Pb^{2+}$ and $Zn^{2+}$, are orthogonal over a wide range of reaction conditions. Sadtler et al. thoroughly investigated partial cation exchange between CdS nanorods and $Cu^+$ ions, and found that the energy of formation of the CdS–$Cu_2S$ interface was minimized when $Cu_2S$ nucleation occurred at the nanorod ends, followed by inward growth.[115] Furthermore, the reaction was kinetically favored at the Cd-rich terminus of the nanorods, so that CdS nanorods with either one or two $Cu_2S$ segments could be synthesized (Figure 10 a). The orthogonal reactivity of CdS and $Cu_2S$ enabled site-selective modification of the $Cu_2S$ domains through cation exchange with $Pb^{2+}$ ions, thereby leaving the CdS domains unreacted, and templating the formation of a variety CdS-PbS nanorod heterostructures (Figure 10 b).[114] Nanorods with alternating CdS and $Ag_2S$ segments were also treated with $Pb^{2+}$ ions, which led to a topologically controlled, site-selective cation exchange with $Ag_2S$, and a multidomain nanostructure with numerous PbS segments embedded in CdS nanorods.

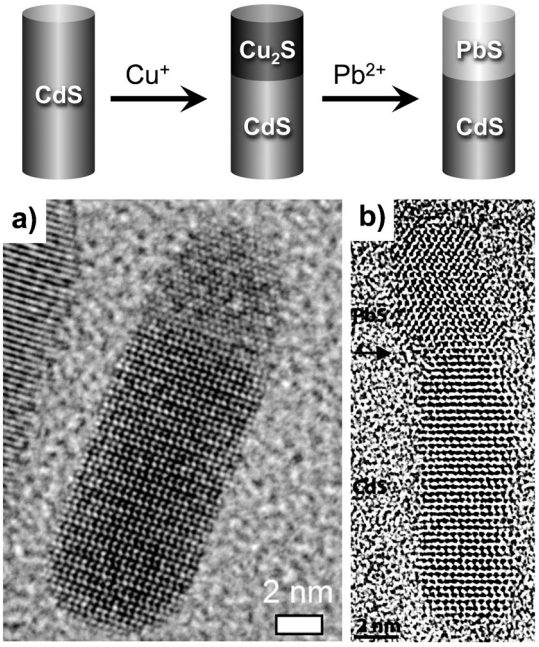


***Figure 10.*** Top: Schematic representation showing the stepwise conversion of a CdS nanorod into a PbS-CdS striped nanorod by two sequential ion-exchange reactions and a $Cu_2S$-CdS nanorod intermediate. HRTEM images of a) a $Cu_2S$-CdS striped nanorod formed by treating CdS nanorods with $Cu^+$ and b) a PbS-CdS striped nanorod formed by treating $Cu_2S$-CdS nanorods with $Pb^{2+}$. Panel (a) reprinted from Ref. [115] with permission (Copyright 2009, American Chemical Society) and panel (b) reprinted from Ref. [114] with permission (Copyright 2009, American Chemical Society).

Heterogeneous seeded-growth reactions are site selective when deposition is favored at a particular location on a seed particle, which may have several sites that could accommodate the addition of a new domain. For example, addition of a nanoparticle to highly faceted or anisotropically shaped seeds can favor growth from a particular area, such as the terminus of a nanorod. Nanocrystals having the hcp wurtzite structure (i.e. Cd*X*, ZnO, ZnS) are routinely grown into highly anisotropic shapes, including nanorods and branched multipods, as a result of incomplete passivation of high-energy (001) surfaces, which results in preferential growth along the *c* axis.[141,142] In the seminal paper by Mokari et al., Au domains were grown site selectively from either one or both ends of CdSe nanorods, which was also explained by the high surface energy and weak ligand adsorption to the (001)-terminated tips.[143] The selectivity was assigned to a mechanism wherein soluble Au complexes were preferentially adsorbed on the CdSe nanorod tips, followed by reduction. Another interesting feature of the wurtzite structure is the lack of inversion symmetry perpendicular to its *c* axis, which renders (001) and (00$\bar{1}$) facets compositionally and energeti-

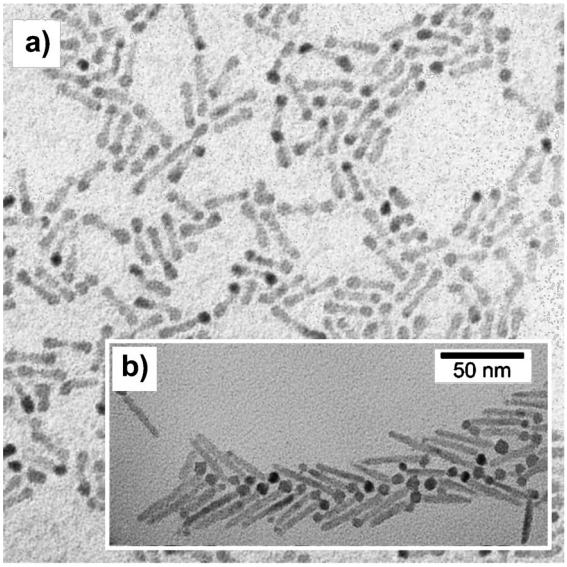


***Figure 11.*** TEM images of CdSe nanorods selectively capped with PbSe at a) both ends (PbSe-CdSe-PbSe) and b) one end (PbSe-CdSe). Reprinted from Ref. [144] with permission (Copyright 2005, American Chemical Society).

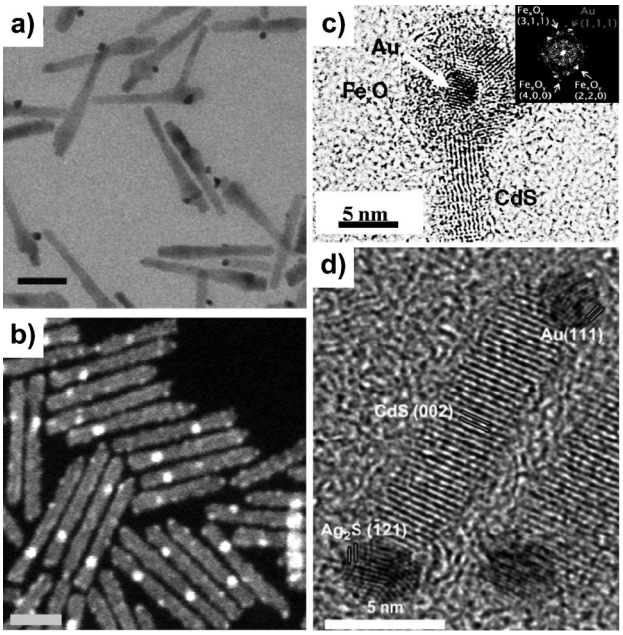


***Figure 12.*** TEM images showing a) Pt nanoparticles photodeposited selectively at the CdSe core region of CdSe/CdS core–shell nanorods (scale bar: 20 nm), b) Au nanoparticles deposited selectively at the CdSe core region of CdSe/CdS core–shell nanorods (HAADF-STEM image, scale bar: 20 nm), c) iron oxide deposited selectively at the Au end of Au-tipped CdS nanorods, and d) Au and $Ag_2S$ selectively deposited at opposite ends of a CdS nanorod (Au-CdS-$Ag_2S$). Panel (a) reprinted from Ref. [146] with permission (Copyright 2008, Wiley-VCH), panel (b) reprinted from Ref. [147] with permission (Copyright 2008, American Chemical Society), panel (c) reprinted from Ref. [149] with permission (Copyright 2010, American Chemical Society), and panel (d) reprinted from Ref. [150] with permission (Copyright 2010, Wiley-VCH).

cally non-equivalent, and implies a driving force for terminus-selective heterogeneous growth from wurtzite-type nanorods. Kudera et al. utilized this non-equivalence to controllably deposit PbSe domains on either one or both tips of CdS and CdSe nanorods (Figure 11).[144] In addition to crystal structure effects, the surface energetics associated with site-selective addition to anisotropic seeds are complicated by many variables, including ligand dynamics, surface curvature, tapering, and epitaxy. This subject has been thoroughly reviewed by Carbone and Cozzoli.[26] Our focus will be on heterogeneous seeded-growth reactions where a new domain was added to a multidomain nanostructure, with an emphasis on site selectivity that was promoted by the heterostructured seed.

The eccentric CdSe/CdS core–rod-shell hybrid nanocrystals developed by Manna and co-workers are an interesting platform for studying site-selective seeded growth from a multidomain nanostructure.[145] Organometallic precursors are decomposed in the presence of CdSe/CdS seeds to make metal–semiconductor nanostructures for charge separation and light-harvesting studies. Dukovic et al. have shown, for example, that photodeposition of Pt onto single-component CdS nanorods resulted in random decoration of the lateral facets with multiple Pt domains. When the CdSe/CdS core–rod-shell structures were used as seeds instead, only one large Pt domain grew, at a location corresponding to the embedded CdSe core (Figure 12a).[146] The authors speculated that photoexcited electrons and holes experienced confinement as a result of a potential minimum in the CdSe domain, which may have influenced the site-selective growth. Similarly, Menagen et al. reported growth of Au domains localized at the buried CdSe core (Figure 12b).[147] Initially, they observed a random decoration of the nanorod side walls with small Au clusters. The tendency of conduction electrons to flow from the CdS domain to the lower-potential CdSe seed caused oxidation of the Au clusters, which increased the likelihood that larger Au domains would grow and persist at the seed position. In a subsequent report by Carbone et al., the tendency for growth to occur near the core region of the seeds was surmounted by assisting $Au^{III}$ reduction with UV photoexcitation, whereby a large, plasmonically active Au domain could be spatially directed toward one end of the CdSe/CdS nanorods.[148] More recently, UV excitation of Au-tipped CdSe/CdS "nano-matchsticks" was used to selectively photodeposit Pd and Fe metal onto the Au domains.[149] Heterogeneous deposition and subsequent oxidation of Fe gave rise to termination of each nanorod with Au/$Fe_xO_y$ yolk–shell domains (Figure 12c), which is similar to what was observed by Schevchenko et al. during thermal decomposition of [$Fe(CO)_5$] over Au seeds.[137] Instead of heterostructured termini, UV photodeposition of Pd resulted in alloying between the Au domains and Pd.[149]

Thermally induced decomposition of [$Co_2(CO)_{10}$] over the dot-in-rod CdSe/CdS seeds generated matchstick-like hybrid nanoparticles, with one Co domain linked selectively to the terminus farthest from the CdSe core.[62] In contrast, replacing the core–rod-shell seeds with single-domain CdS nanorods resulted in random decoration of the lateral side walls with

  

Co. Site-selective Co growth was rationalized on the basis of a difference in the permanent dipole moment (arising from asymmetry perpendicular to the wurzite *c* axis) between the CdSe/CdS core–shell seeds and pure CdS nanorods, which potentially originated from lattice strain around the CdSe–CdS interface. Furthermore, single-domain Co nanocrystals synthesized under identical control conditions had the cubic ε-Co crystal structure, but Co-CdSe/CdS matchsticks contained hcp-Co, presumably from adjoining to the hcp-CdS apex. Synergistic interaction at the heterojunction between Co and CdS also gave rise to unexpected ferromagnetism at room temperature.

Chakrabortty et al. studied the reduction of $Au^{III}$ salts in the presence of CdSe/CdS core–rod-shell seeds, and reported site-selective deposition of Au domains through systematic variations in the precursor concentration.[150] At low $Au^{III}$ concentrations, Au-CdSe/CdS with a matchstick hybrid structure was obtained, with the Au domain located at the nanorod tip farthest from the CdSe core, similar to the deposition of Co. The formation of the substrate core–shell nanorods results from heterogeneous nucleation of CdS over CdSe seeds, followed by kinetically favored growth of the $(00\bar{1})$ facets, which are terminated primarily by sulfur atoms. (The (001) face is Cd rich.) Au-CdSe/CdS nanomatchsticks likely resulted from rapid attachment of Au atoms to the S-rich $(00\bar{1})$ face, but only at low precursor concentrations. Systematically increasing the $Au^{III}$ concentration gave rise to symmetrically tipped Au-CdSe/CdS dumbells and, above a threshold concentration, to random decoration. Notably, many randomly decorated nanorods had one larger Au domain co-located with the CdSe core, consistent with aforementioned reports. Replacing $Au^{III}$ with similarly low concentrations of $Ag^{I}$ induced site-selective cation exchange at one end of the nanorod, thereby forming $Ag_2S$-CdSe/CdS matchsticks. The high degree of selectivity in Au and $Ag_2S$ growth enabled CdSe/CdS nanorods to be reacted sequentially with $Au^{III}$ and then $Ag^{I}$, thus leading to asymmetrically tipped $Ag_2S$-CdSe/CdS-Au dumbbell-like hybrid nanoparticles with four distinct inorganic domains (Figure 12d).

To reduce the lattice mismatch induced strain that can lead to interfacial defects and charge-carrier trap states in core–shell nanocrystals, seeded-growth reactions have been carried out sequentially to grow multiple, concentric shells around a nanocrystal core. Even for core–shell systems with a modest lattice mismatch, such as CdSe/CdS (3.9%), growth of more than two monolayers of shell material introduces significant strain.[151] In "onion-like" nanostructures with a core and several shells, multiple heterojunctions extend radially from the center. These heterojunctions are characterized by a gradient of gradually increasing lattice mismatch and band-gap offset, thereby allowing the growth of thicker shells that more adequately confine excitons within the core. Examples of core–multishell nanostructures prepared by stepwise seeded growth include InAs/CdSe/ZnSe,[152] CdSe/CdS/ZnS,[153–155] and the quantum-dot-well-dot system CdS/HgS/CdS.[156,157] Similarly, Xu et al. deposited multiple metallic shells around a magnetic $Fe_3O_4$ core in a sequential manner.[158] The growth of thicker Au shells from $Fe_3O_4$/Au core–shell seeds resulted in a red-shift of the visible absorbance as a result of surface plasmon resonance (SPR), while growth of an Ag shell led to the formation of $Fe_3O_4$/Au/Ag core–multishell structures that caused a blue-shift of the SPR band.

When compared to situations in which core–shell seeds are used, heterogeneous seeded-growth reactions become more complex when the substrate seeds possess multiple, chemically distinct surfaces that are exposed to the surrounding growth solution. For example, in a situation where two-component heterodimers are utilized as seeds, from which surface does the third component grow, and why? Although complex mixtures of multicomponent products might be expected in such reactions, heterogeneous nucleation is often favored at one particular surface. One of the first examples involved the growth of lead chalcogenide domains from heterodimer Au-$Fe_3O_4$ seeds, which formed ternary colloidal hybrid nanoparticles with unprecedented semiconducting–metallic–magnetic functionality (Figure 13a,b).[159,160] Heterogeneous nucleation of lead chalcogenides always occurred site-selectively at the Au surface, and never at $Fe_3O_4$, thus giving rise exclusively to multidomain nanoparticles with PbX-Au-$Fe_3O_4$ (X = S, Se) connectivity. The authors proposed that site-selective addition of PbS domains was driven by rapid adsorption of S atoms onto the solvent-exposed Au surfaces, and the subsequent reaction of those S atoms with the Pb–oleate precursor complex.[159] Clear mechanistic differences between the reaction of the Pb–oleate complex with the sulfur and selenium (trialkylphosphine–selenium complex, TOP-Se) precursors suggested that a different driving force was responsible for heterogeneous nucleation of PbSe.[160] Several experiments suggested that Au-$Fe_3O_4$ seeds simply provide a low-energy Au surface onto which small PbSe nuclei attach, coalesce, and grow. The PbSe morphology was controllable by varying the Au-$Fe_3O_4$ to Pb-oleate (seed-to-precursor) ratio, with higher seed-to-precursor ratios giving rise to spherical PbSe domains, and lower ratios generating rod-shaped PbSe domains. When single-component Au nanoparticles were used as seeds over a broad range of seed-to-precursor ratios, however, Au/PbSe hybrid particles with a core–shell morphology formed, and rod-shaped PbSe domains were not observed. Remarkably, nanorod-shaped PbSe growth occurred because of the presence of the $Fe_3O_4$ domain, which limited the surface area of Au that was exposed, and that could accommodate the nucleation of PbSe. This ensured that significant quantities of Pb and Se precursor remained available post-nucleation, which is consistent with anisotropic growth and the resultant rodlike domains. Furthermore, even lower concentrations of Au-$Fe_3O_4$ seeds resulted in PbSe domains with multiple, rodlike, and branched domains.

In a way that is analogous to the synthesis of organic molecules, a particular sequence of transformations is often required to construct a multidomain nanostructure with a targeted morphology or connectivity. The order in which sequential seeded-growth additions are carried out has a profound effect on whether or not site-selective heterogeneous nucleation is observed. Colloidal hybrid Ag-Au-$SiO_2$ nanoparticles, for example, were formed by partial encapsulation of spherical Au nanoparticles in silica, followed by site-

  

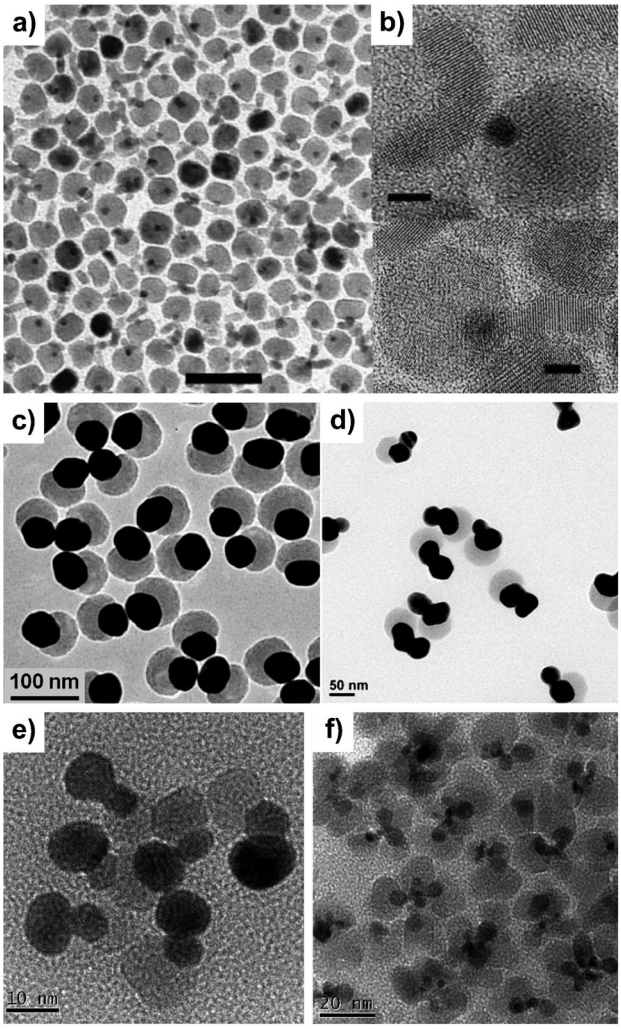


***Figure 13.*** TEM images of a,b) PbSe nanorods grown selectively off the Au domain of Au-$Fe_3O_4$ heterodimers to generate PbSe-Au-$Fe_3O_4$ heterotrimers, c) Au-$SiO_2$ heterodimers and d) Ag-Au-$SiO_2$ heterotrimers formed by growing Ag selectively off the Au domains, and e,f) various Au-Pt-$Fe_3O_4$ heterotrimers formed by the selective growth of e) Au off the Pt domains of Pt-$Fe_3O_4$ heterodimers and f) $Fe_3O_4$ off the Au domains of Au-Pt heterodimers. Panels (a,b) reprinted from Ref. [160] with permission (Copyright 2006, Wiley-VCH), panels (c,d) reprinted from Ref. [161] with permission (Copyright 2010, American Chemical Society), and panels (e,f) reprinted from Ref. [163] with permission (Copyright 2008, American Chemical Society).

selective growth of Ag from the Au surface that remained exposed (Figure 13c,d).[161] Partial encapsulation was facilitated by two ligands, 4-mercaptophenylacetic acid (4-MPAA) and poly(acrylic acid) (PAA), which competed with each other to replace native citrate ligands on the Au surface. The portion of the Au surface coated in 4-MPAA was amenable to encapsulation with silica, and the PAA-terminated surface was not, thus resulting in partial encapsulation. (Note that the reactivity of 4-MPAA- and PAA-functionalized Au surfaces are *orthogonal* with respect to silica deposition.) The resulting Ag-Au-$SiO_2$ connectivity would have been nearly impossible to obtain if Ag was first deposited onto Au, followed by silica growth. First of all, the deposition of Ag onto Au seeds typically results in core–shell structures, because of the similar lattice constants of Au and Ag. Notably, the nonconcentric morphology obtained here gave rise to a new SPR band at 674 nm, in addition to the visible SPR bands arising from Au and Ag at 525 and 405 nm. This band was assigned to longitudinal plasmon coupling between the Au and Ag domains. Secondly, site-selective encapsulation of Au in the presence of Ag is unlikely because Au and Ag colloids can both accommodate the growth of a silica shell.[162]

Zhang et al. studied various sequences of seeded-growth reactions involving Pt, Au, and $Fe_3O_4$, and obtained a wide variety of ternary morphologies (Figure 13e,f).[163] Multidomain nanostructures comprised of branched Pt nanorods with either one or multiple tips made of Au were used as seeds for the addition of $Fe_3O_4$ domains by thermal decomposition of $[Fe(CO)_5]$. The final morphology of the Pt-Au-$Fe_3O_4$ heterostructures was ascribed to variation in the decomposition rate of $[Fe(CO)_5]$, which was dependent on its concentration and the reaction temperature. Provided that the temperature and precursor-to-seed ratio were sufficiently low, the growth of $Fe_3O_4$ site-selectively added to either one or multiple Au domains when they were below a certain size. In contrast, encapsulation of the branched Pt domains with $Fe_3O_4$ was favored when the Au domains were relatively large. Above a threshold concentration of $[Fe(CO)_5]$, or above a threshold temperature, the Au-Pt seeds were completely encapsulated by $Fe_3O_4$. When preformed Pt-$Fe_3O_4$ heterodimers were used as seeds instead, Au domains grew site selectively from the Pt surface, and not from $Fe_3O_4$, which demonstrated that the order of reactions plays a significant role in determining the heterostructure morphology.

Just as seeded growth represents a transformational analogue of organic addition reactions for the bottom-up construction of inorganic nanostructures, elimination reactions correspond to the top-down modification of multicomponent nanostructures through deconstruction. This is accomplished using oxidizing agents that either partially or completely dissolve one or more components in a site-selective manner. One prominent example, termed "on-wire lithography", involved wet-chemical etching of template-grown striped nanowires with either alternating Au-Ag or Au-Ni segments (Figure 14a).[164] Selective elimination of Ag or Ni was accomplished by treatment with either $HNO_3$ or a methanolic solution of $H_2O_2$ and $NH_4OH$, respectively, which left Au segments intact. The striped nanowires were thereby transformed into arrays of Au disks, separated by size-tunable gaps perpendicular to the longitudinal nanowire axis. Insulating gaps in an otherwise conductive nanowire are an interesting platform for studying gap functionalization and its effect on electrical transport,[165] surface-enhanced Raman scattering (SERS),[166] and biomolecular sensing.[167] Another demonstration of selective dissolution involved the use of multiply twinned Ag nanoparticles as morphological templates, and resulted in remarkable, thin ($<2$ nm) nanoframes of Au (Figure 14b).[168] Under optimized conditions, $HAuCl_4$ was reduced with ascorbic acid, selectively depositing Au onto the edges and corners of decahedral Ag nanoparticles. Hydrogen peroxide solution was then used to dissolve the Ag component, leaving decahedral Au nanoframes behind.

  

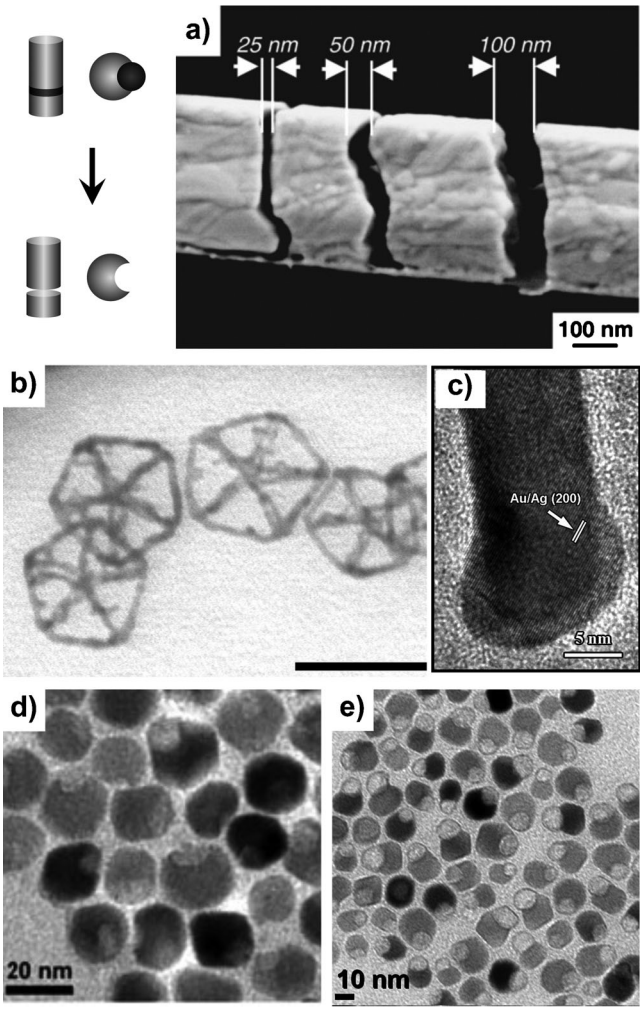


***Figure 14.*** Top left: Schematic represention of nanoscale elimination reactions by selective dissolution. a) FESEM image of an Au nanowire with 25, 50, and 100 nm gaps created by selectively dissolving the Ni components of Au-Ni multisegmented nanowires. TEM images of b) Au nanoframes formed by facet-selective overgrowth of Au on decahedral Ag nanoparticles and selective dissolution of Ag (scale bar: 50 nm), c) Ag-tipped Au nanorods formed by selectively etching Ag from the sides of Au@Ag core–shell nanorods, d) dented $Fe_3O_4$ nanoparticles formed by selectively dissolving the Au domains of Au-$Fe_3O_4$ heterodimers, and e) $Fe_3O_4$ nanocontainers formed by selectively dissolving the Au domain of Au-$Fe_3O_4$ heterodimers with additional $Fe_3O_4$ covering the Au. Panel (a) reprinted from Ref. [164] with permission (Copyright 2005, American Association for the Advancement of Science), panel (b) reprinted from Ref. [168] with permission (Copyright 2011, American Chemical Society), panel (c) reprinted from Ref. [170] with permission (Copyright 2012, American Chemical Society), panel (d) reprinted from Ref. [171] with permission (Copyright 2010, Wiley-VCH), and panel (e) reprinted from Ref. [172] with permission (Copyright 2011, American Chemical Society).

Other faceted Ag nanoparticles, such as pentagonal nanorods and icosahedra, were also viable templates for the formation of the Au nanoframe. Notably, the same techniques have also been used to selectively de-alloy a target metal from bimetallic alloy nanoparticles, such as the dissolution of Ag from AuAg alloy nanostructures.[169]

Recently, selective dissolution of Ag from the lateral side walls of Au/Ag core–shell nanorods resulted in dumbbell-like nanostructures with Au/Ag core–shell domains remaining only at the tips (Figure 14c).[170] Metallic Ag was oxidized using $Fe^{3+}$ ions, and cetyltrimethylammonium bromide (CTAB) surfactant promoted etching by strongly ligating to $Ag^+$. Silver atoms along the lateral facets were oxidized faster than those at the nanorod tips, which contradicted previous studies pertaining to wet chemical etching of pure Au nanorods. The adsorption of CTAB to the nanorod side walls, which correspond to {110} crystal facets for fcc metals, was expected to impart favored reaction kinetics at the tips. Zeta potential measurements and thermogravimetric analysis indicated that the CTAB populates the surface of Au/Ag core–shell nanorods to a much lower extent than pure Au nanorods. It was, therefore, concluded that the rate of Ag dissolution was proportional to intrinsic surface energies (for fcc, $110 > 100 > 111$). The Ag-tipped Au nanorods exhibit higher catalytic activity toward the room-temperature reduction of *p*-nitrophenol than either Au/Ag core–shell or pure Au nanorods, which the authors ascribed to an electronic synergetic effect between Au and Ag. Similarly, selective elimination of either Au or $Fe_3O_4$ from Au-$Fe_3O_4$ heterodimers was used to demonstrate that Au-$Fe_3O_4$ particles exhibit a synergetic enhancement in catalyzing the reduction of $H_2O_2$.[171] Single-component Au and $Fe_3O_4$ nanoparticles were obtained by dissolving either the Au domain using $KI/I_2$ solution, or the $Fe_3O_4$ domain with $H_2SO_4$ (Figure 14d). The authors were then able to compare the catalytic activity of Au, $Fe_3O_4$, and the parent Au-$Fe_3O_4$ heterodimers separately and under identical conditions.

Selective etching of Au with $I_2$ was also demonstrated by George et al., who eliminated the Au domain from a series of asymmetric core–shell and Au-$Fe_3O_4$ heterodimers (Figure 14e).[172] Thermal decomposition of $[Fe(CO)_5]$ in the presence of Au nanoparticles at 180–200 °C results in slow seeded growth of $Fe_3O_4$ shells. Increasing the temperature, however, causes the core and shell to become increasingly noncentrosymmetric, and eventually the Au and $Fe_3O_4$ surfaces spatially segregate into the heterodimer morphology. The authors found that $I_2$ molecules selectively leached Au from either the asymmetric core–shell Au/$Fe_3O_4$ particles or the Au-$Fe_3O_4$ heterodimers, while the remaining $Fe_3O_4$ domain remained morphologically unchanged. The core–shell domains were transformed into porous shells with a large internal void space (so-called nanocontainers), while the heterodimers evolved into nanoparticles with a large concave region. Inorganic structures that mimic containers are desirable for applications that require the storage and controlled release of guest species, and the authors showed that the cavity of "dense $Fe_3O_4$–shell $Fe_3O_4$" hybrid nanocontainers could indeed be loaded with the molecular anticancer agent cisplatin. After coating the cisplatin-loaded dense $Fe_3O_4$–shell $Fe_3O_4$ nanocontainers with a polymer to confer water dispersability, ultrasonication was applied to rupture the porous shell-like domain, thereby releasing the drug into solution. Selective etching of Au with $I_2$ was also carried out on AuPt-$Fe_3O_4$ heterostructures, which deconstructed the AuPt domains by completely leaching Au, thus

leaving small (1–3 nm) Pt domains trapped within the void space or concave region. The Pt/$Fe_3O_4$ nanocontainers were efficient photocatalysts for reduction of an organic dye, and were magnetically recoverable from the product mixture.

### 4.2. Piecewise Merging of Multidomain Nanostructure Fragments: "Coupling" Reactions

Chemists frequently link together smaller molecular fragments through coupling reactions to construct large molecules. Similarly, reactions that link nanoparticles into higher-order hybrid structures have the potential to significantly expand our ability to design and synthesize larger multidomain nanostructures in a predictable manner. As an example, Gao et al. used a nanoscale soldering technique to weld multisegmented nanowires together, with an emphasis on environmentally friendly "lead-free" compositions.[173] The terminal segment(s) of each striped nanowire was made of Sn solder, which aided joint formation between striped nanowires when heated in a liquid under agitation. Various combinations of nanowires with multiple segments of Au, Ni, and Sn were thereby merged into complex multisegmented networks, which could be an interesting technique for fabricating electronic devices that require robust and electrically conductive interconnects.

Several examples of solid-state coupling for colloidal hybrid nanoparticles involved the solution-mediated merging and thermal sintering of solvent-exposed Au domains. For example, Au-$Fe_3O_4$ heterodimers were heated in the presence of trace amounts of sulfur, which caused the Au to coalesce into a single domain, thereby bringing two or three $Fe_3O_4$ domains together (Figure 15a).[159] The coupling of Au-$Fe_3O_4$ heterodimers into higher-order oligomers was only observed if sulfur was added to the reaction mixture. Spontaneous adsorption of sulfur atoms was responsible for displacing the hydrophobic surface ligands from Au, which colloidally destabilized and drove the aggregation of the Au domains in nonpolar media. Our research group utilized this strategy to couple linear heterotrimers of Au-Pt-$Fe_3O_4$, and obtained a variety of oligomer-type hybrid structures with as few as two and as many as six heterotrimers bridged by fused Au domains.[174] The Au domains were significantly larger in the Au-Pt-$Fe_3O_4$ heterotrimers than in Au-$Fe_3O_4$ (approximately 8 nm in Au-Pt-$Fe_3O_4$ compared to 2 nm in Au-$Fe_3O_4$), however, which resulted in incomplete, partial diffusion of the coupled Au domains, and a random distribution of morphologies. It is, therefore, reasonable to assume that these coupling processes are optimized when the solid–solid diffusion distances are minimized, and the surface areas are small enough to self-regulate the morphological outcome (e.g. when the domains that promote coupling are small).

Metal–semiconductor networks of alternating Au dots and CdSe nanorods were obtained by heating dumbbell-shaped Au-CdSe-Au hybrid nanoparticles in the presence of a trace amount of molecular $I_2$ (Figure 15b–d).[175,176] The role of $I_2$ is to destabilize the Au surface, thereby leading to controlled aggregation, and is therefore similar to the role of trace amounts of sulfur. The chainlike networks were

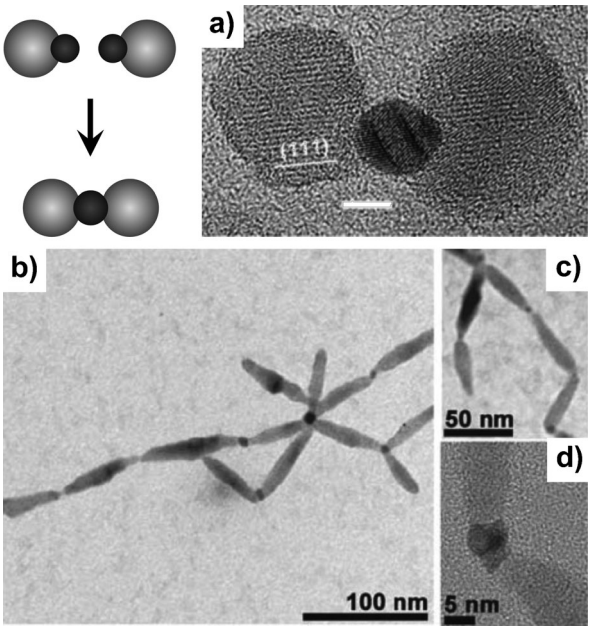


***Figure 15.*** Top left: Schematic represention of hybrid nanoparticle coupling reactions. TEM images of a) $Fe_3O_4$-Au-$Fe_3O_4$ heterotrimers formed by heating Au-$Fe_3O_4$ heterodimers with trace amounts of sulfur and b–d) linear $(Au\text{-}CdSe)_n$ chains formed by treating Au-CdSe-Au nanorods with $I_2$. Panel (a) reprinted from Ref. [159] with permission (Copyright 2006, American Chemical Society) and panels (b–d) reprinted from Ref. [176] with permission (Copyright 2009, Wiley-VCH).

dielectrophoretically assembled into devices that were designed to measure voltage–current response. Thermal annealing of the devices caused (as-made) CdSe nanorods that were randomly decorated with small Au nanoparticles to undergo a rearrangement in morphology, which was monitored in a previous study by using in situ TEM.[177] Au atoms and small Au clusters diffused along the lateral nanorod facets upon heating and coalesced at the Au-CdSe heterojunctions to form much larger Au domains. In contrast to the randomly decorated Au-CdSe components, which formed kinetically during low-temperature deposition of Au, the annealed heterostructure possessed high-quality, epitaxially well-defined Au-CdSe interfaces with increased interfacial area, which is important for the application of such metal–semiconductor nanostructures to electronics.

Teranishi et al. demonstrated that incomplete surface passivation, similar to the destabilization of Au domains by sulfur atoms or $I_2$, leads to the solid-state coupling of hybrid nanoparticles. Seeded growth of $Co_9S_8$-$PdS_x$ heterodimers was accomplished by treating $[Co(acac)_2]$ with 1-octadecanethiol in the presence of $PdS_x$ seeds (Figure 16a–d). At long reaction times, however, the dominant product consisted of two $PdS_x$ domains bridged by $Co_9S_8$, thus resulting in a three-domain, peanut-shaped morphology.[178] Since 1-octadecanethiol behaved as a surface-stabilizing ligand, but was also consumed in the reaction with $[Co(acac)_2]$, the authors ascribed the formation of $PdS_x$-$Co_9S_8$-$PdS_x$ heterostructures to the diffusion-mediated coalescence of $Co_9S_8$ domains, driven by insufficient surface passivation. Increasing the concentration of alkanethiol in the reaction mixture suppressed coupling,

  

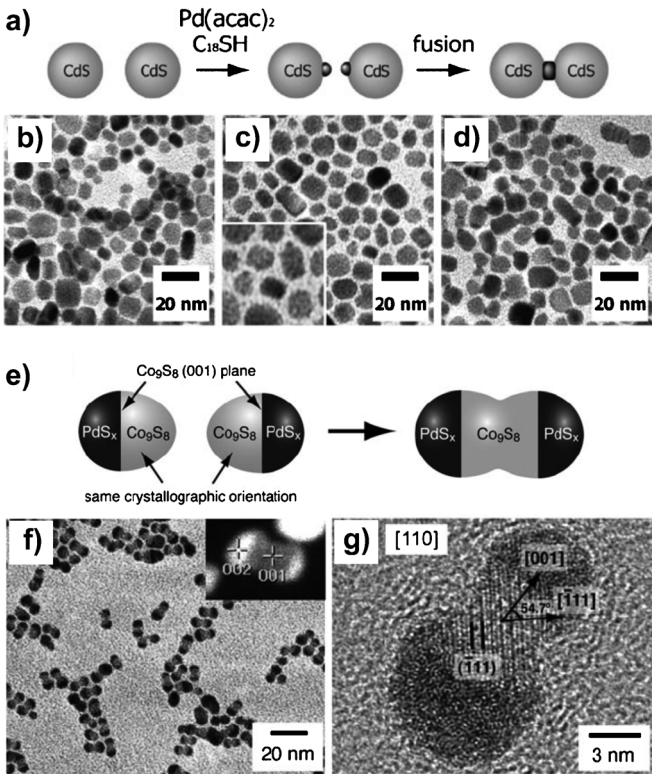


***Figure 16.*** a) Schematic representation and b–d) corresponding TEM images showing the formation of CdS-$PdS_x$-CdS hybrid particles by installing a $PdS_x$ domain on b) CdS nanoparticles to form c) CdS-$PdS_x$ dimers, followed by fusion to form d) the CdS-$PdS_x$-CdS products. e) Schematic representation and corresponding f) TEM and g) HRTEM images of $PdS_x$-$Co_9S_8$-$PdS_x$ hybrid particles formed from the fusion of the $Co_9S_8$ domains on $PdS_x$-$Co_9S_8$ dimer particles. Panels (a–d) reprinted from Ref. [178] with permission (Copyright 2009, The Royal Society of Chemistry) and panels (e–g) reprinted from Ref. [179] with permission (Copyright 2007, Wiley-VCH).

and the acorn-shaped $Co_9S_8$-$PdS_x$ heterodimers were then the dominant morphological product. Similarly, rodlike CdS domains were bridged through the thermally induced coupling of CdS-$PdS_x$ heterodimers, with formation of dumbbell- and flower-shaped CdS-$PdS_x$ heterostructures through the fusion of $PdS_x$ domains (Figure 16e–g).[179]

### 4.3. Protection/Deprotection Strategies

Protective groups enable site-selective modifications to be carried out on molecules that possess multiple reactive centers. Temporary shielding of targeted functional groups creates orthogonally reactive sites within a molecule, which facilitates transformation of the unprotected groups. Although protection/deprotection sequences are ubiquitous in organic synthesis, the deliberate application of such strategies to building inorganic nanostructures remains largely unexplored. One simple example was discussed in a previous section, where the fabrication of Au nanodisk arrays with size-tunable gaps was achieved by selectively eliminating Ag and Ni segments that were susceptible to dissolution.[164] Before the wet-etching step, the striped nanowires were dispersed onto a glass substrate, and a corrosion-resistant coating of either $SiO_2$ or an Au/Ti bilayer was applied. The nanowire side walls that were facing up became coated, and the side walls that were in contact with the substrate were physically protected. This protection scheme allowed the half-exposed Ag and Ni segments to be etched away in the next step, while the corrosion-resistant layer provided structural support to the Au nanodisk array.

Our research group used electrochemically deposited nanowires to demonstrate a similar physical protection scheme (Figure 17).[180] Electrodeposition of metal nanowires involves the use of a rigid, insulating template such as porous polycarbonate or anodic aluminum oxide (AAO) membranes, which require one of their sides to be coated with conductive metal. Template-confined Pt nanowires were treated with a variety of metal salts under reducing conditions to induce site-selective transformation into intermetallic phases (PtPb, PtBi, PtSn, PtCo). The metallurgical diffusion reactions were forced to begin at the tips and proceed inward, because the membrane provided physical protection to the side walls. This physical constraint allowed us to partially modify multi-segmented nanowires in a rational, stepwise fashion, by using reaction parameters that control the diffusion rate and distance (concentration, temperature, reaction time).[107] Two-component Pt-Ni nanowires were reacted partially with trioctylphosphine to form Pt-Ni-$Ni_2P$, and then reacted partially with $Pb(CH_3COO)_2$ to make four-component $PtPb_x$-Pt-Ni-$Ni_2P$ nanowires (Figure 17a). One terminus of the template-confined nanowires could also be reacted selectively, by making use of the conductive backing layer as a protective group.

Oxidative etching of CTAB-functionalized Au nanorods is a convenient approach for lowering their aspect ratio, because dissolution is favored at the nanorod ends, which enables facile tuning of the longitudinal SPR absorbance.[181] The site-selective nature of this transformation implies that transverse oxidation of Au nanorods should be challenging. Bao et al. devised a chemical protection scheme to surmount the chemoselective barrier, by selectively depositing protective $Ag_2O$ domains onto Au nanorod tips.[182] Oxidation was prevented from occurring at these sites, and instead produced dimples and significant roughening along the side walls of the Au nanorod, which are interesting features for SPR. A controllable red-shifting of the longitudinal SPR band by up to 250 nm was achieved by varying the etching time.

Chemical protection was also applied to the transformation of colloidal nanocrystals to synthesize quasi-hemispheric metallic particles that feature a deep cavity, or "nanobowls".[183] The heterodimer Ag-$Fe_3O_4$ nanoparticles were treated with AuCl, which induced oxidation and galvanic replacement of Ag atoms with Au. The authors proposed that the key process was formation of a uniform Au shell around the Ag domain, thereby excluding the portion of the Ag surface that was adjoined to and protected by the $Fe_3O_4$. Subsequent detachment of the Ag/Au core–partial-shell domain from the $Fe_3O_4$ protecting group allowed Ag ions that initially formed bonds with the $Fe_3O_4$ to be ejected from the nanocrystal, along with concomitant thickening of the Au shell. This process resulted in enlargement of the interior

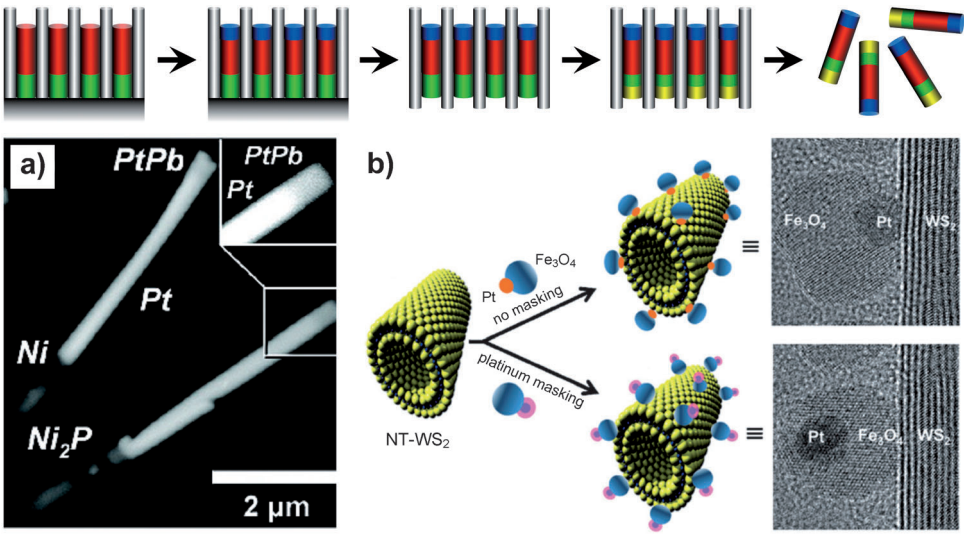


***Figure 17.*** Top: Schematic representation of the synthesis of asymmetrically tipped striped metal nanowires synthesized by stepwise chemical conversion within an anodic aluminum oxide membrane using a physical protection/deprotection strategy. a) SEM image of four-component striped $Ni_2P$-Ni-Pt-PtPb nanowires synthesized as shown in the schematic representation. b) Schematic representation and corresponding TEM images of domain-selective binding of Pt-$Fe_3O_4$ heterodimers to $WS_2$ nanotubes by molecular surface modification. Panel (a) reprinted from Ref. [107] with permission (Copyright 2009, American Chemical Society) and panel (b) reprinted from Ref. [184] with permission (Copyright 2011, Wiley-VCH).

cavity and of the particle diameter. The authors also demonstrated that the nanobowls could carry cargo by depositing small Au nanoparticles inside the cavities.

A final example of chemical protection enabled manipulation of the hierarchical assembly of colloidal Pt-$Fe_3O_4$ heterodimers on the surface of $WS_2$ nanotubes (Figure 17b).[184] Sahoo et al. showed without the use of protective groups that Pt-$Fe_3O_4$ heterodimers were oriented with Pt domains attached to $WS_2$ and the magnetic domains faced outward. This chemoselectively driven attachment was ascribed to favorable soft–soft acid–base interactions, based on Pearson's hardness, between Pt and the sulfur-rich $WS_2$ surface. A protective layer of sterically bulky, thiol-terminated ligands [*O*-[2-(3-mercaptopropionylamino)ethyl]-*O*′-methylpolyethylene glycol 5000; (SH-PEG-$OCH_3$)] was then applied to the Pt domains, which reversed the directionality of assembly, presumably by diminishing the effect of those soft–soft interactions. After replacing the native surface ligands on Pt (oleic acid, oleylamine) with the protective SH-PEG-$OCH_3$, attachment to $WS_2$ occurred almost exclusively through the $Fe_3O_4$ domain.

These reports demonstrate the applicability and versatility of protection strategies to nanostructure synthesis, and many more examples are expected to emerge. Ultimately, protection/deprotection strategies could help to facilitate the controlled placement of nanoparticles into any desired, arbitrary sequence, thereby leading to hybrid nanoparticle analogues of molecular isomers, each with distinct heterojunctions and materials linkages that have an impact on the properties, such as the direction of electron transfer, the selectivity of a catalytic reaction, and the coupling of surface plasmons.

## 5. Stepwise Construction of High-Order Multicomponent Inorganic Nanostructures

When the synthetic tools and concepts outlined in the preceeding sections are integrated, a "total synthesis" concept emerges for the predictable construction of large molecules built from smaller molecular fragments. Such an approach follows naturally from the available functional groups, the large library of chemical reactions, and strategies that facilitate their implementation in a logical manner. The availability of nanoparticle "synthons", a growing library of chemical reactions that support predictable modifications of nanoparticles, and demonstrations of orthogonal reactivity, site selectivity, protection/deprotection collectively suggest that a similar approach may be viable for constructing higher-order multicomponent inorganic nanostructures. Indeed, a total synthesis concept for multicomponent nanostructures has the potential to permit chemists to respond to increasingly stringent and sophisticated design criteria for functional nanomaterials. The efficient harvesting of sunlight for the renewable production of solar fuels and electricity, for example, is one of the most significant demand-driven pursuits in modern research,[185] and relies critically on our ability to synthesize nanostructures by design. Acharya et al. explain that by-design semiconductor materials must efficiently absorb solar photons and convert the energy into long-lived charge-separated states, but the ground state must also be regenerated at a rate that competes with oxidation and degradation of the light absorber, because of electron vacancies (holes) that remain in the valence band. To this end, the authors designed a colloidal hybrid nanostructure with the ability to localize holes efficiently in one of its domains, at potentials that promoted hole transfer to ligands in the surrounding medium.[55]

Known seeded-growth reactions have been carried out in a stepwise fashion (Figure 18a–d) to generate a ZnSe/CdS core–rod-shell nanocrystal with a metallic Pt domain at the end farthest from the ZnSe. The four-step synthesis required ultrathin CdS shells to be deposited onto preformed ZnSe seeds, followed by unidirectional seeded growth of the rod-shaped CdS domains and site-selective addition of Pt tips. Collectively, the band structures of the adjoined components form an energy gradient that permits transfer of photogenerated electrons in the CdS nanorod to the Pt domain, and for holes to localize in the ZnSe core. Photogenerated holes

  

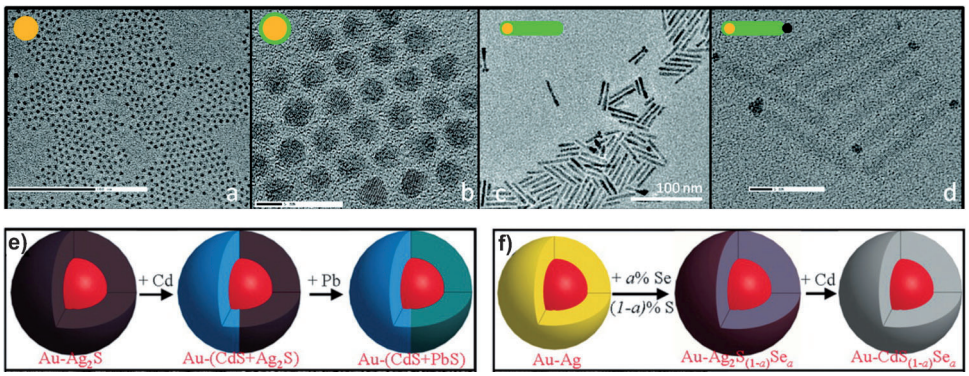


***Figure 18.*** a–d) TEM images showing a four-step synthesis of colloidal ZnSe-CdS-Pt nanorods: a) ZnSe seed nanoparticles, b) ZnSe nanoparticles coated with a thin layer of CdS, c) ZnSe/CdS nanorods grown off the ZnSe/CdS core–shell nanoparticles, and d) ZnSe-CdS-Pt nanorods after site-selective Pt deposition. e,f) Schematic representations of multistep routes to core–shell nanoparticles with controlled metal, anion, and cation compositions. Panels (a–d) reprinted from Ref. [55] with permission (Copyright 2011, American Chemical Society) and panels (e,f) reprinted from Ref. [189] with permission (copyright 2010, American Association for the Advancement of Science).

transferred to the lower-energy ZnSe domain were consequently reduced by electron-donating ligands, namely mercaptoundecanoic acid (MUA) or mercaptopropionic acid (MPA). Localized hole transfer was evidenced by complete quenching of the photoluminescence in the intermediate ZnSe/CdS core–rod-shell "seeds", and after seeded growth of Pt, the hybrid nanostructures were able to generate $H_2$ fuel from the catalytic photoreduction of water. Hydrogen production was sustainable for long periods of time, provided that the solution was periodically regenerated with fresh electron-donating ligands. Notably, isomorphological hybrid nanocrystals with a ZnTe core, where the valence band energy is roughly 0.3 eV above the highest occupied molecular orbital (HOMO) energy of MUA and MPA, did not produce $H_2$.

Seeded growth of an inorganic shell, specifically for luminescent quantum dots, was an innovation designed to mitigate performance losses associated with under-coordinated atoms and imperfections at the surface of a nanocrystal core.[186,187] An engineered core–shell band structure effectively separates exciton wavefunctions in the core from the nanocrystal surface, thereby leading to enhanced quantum emission yields and stability. This approach is limited by epitaxy between the core and shell material, however, because seeded growth of more than a few atomic layers creates mismatch-induced strain, which leads to grain boundaries, dislocations, and other defects. Such imperfections create trap states that are deleterious to performance and, ideally, shell materials should be thick and defect-free.[188] An impressive three-step synthesis addressed this demand, and generated a variety of metal–semiconductor core–shell nanocrystals with high-quality, thickness-tunable, single-crystalline shells (Figure 18e,f).[189] First, a crystalline Ag shell was deposited over a metallic (Au, Pt, FePt, Pd) core by heterogeneous seeded growth, and subsequently converted by oxidative diffusion into amorphous $Ag_2X$ (X = S, Se, Te). The amorphous $Ag_2X$ domain then served as a starting point for cation exchange, which generated the single-crystalline $M_nX_y$ (M = Cd, Zn, Pb) shells, thus enabling the authors to deposit thick, single-crystal shells directly in core–shell systems with significant lattice mismatch. Importantly, the thermodynamics of cation exchange were mediated by Pearson's hard–soft acid–base interactions at the nanocrystal surface and in the surrounding medium, which was the key to accessing single-crystal shells, independently of the crystallinity or structure of the core. The authors also found reaction conditions that allowed the amorphous $Ag_2S$ shells to react partially with $Cd^{2+}$, which was followed by cation exchange of the remaining $Ag^+$ with $Pb^{2+}$ ions. The resulting nanostructures were two-domain shells of CdS/PbS in a ratio of approximately 50:50 surrounding a spherical Au core, which is an important demonstration of compositional engineering at the nanoscale (Figure 18e). Compositional control of the anionic component within the shell domain was also achieved by treating the intermediate Ag shells with a predetermined ratio of sulfur and selenium complexes in the oxidative diffusion step. Amorphous $Ag_2S_{(1-a)}Se_a$ shells with a controllable ratio $a$ were then treated with $Cd^{2+}$, which resulted in single-crystal shells of a ternary $CdS_{(1-a)}Se_a$ alloy (Figure 18f).

Our research group has been working to develop a synthetic concept for constructing multidomain nanostructures that conceptually parallels the total synthesis concept used by organic chemists to prepare complex molecules (Figure 19a–d). Recently, we discovered that a nanoparticle analogue of molecular chemoselectivity is a strong, materials general driving force for establishing connectivity in colloidal hybrid nanoparticles.[174] We studied the addition of transition-metal (M = Au, Ag, Ni, and Pd) domains to heterodimer Pt-$Fe_3O_4$ seeds, which have two chemically distinct surfaces from which M could have conceivably grown. At the outset, we predicted that a mixture of hybrid nanoparticle products with M-Pt-$Fe_3O_4$, Pt-$Fe_3O_4$-M, and M-Pt-$Fe_3O_4$-M heterojunctions was the most likely outcome, because both Pt-M and M-$Fe_3O_4$ hybrid nanoparticles are stable and can be made under similar conditions. Instead, each reaction gave rise to three-component heterotrimers with only M-Pt-$Fe_3O_4$ linkages, where Au, Ag, Ni, and Pd all grew exclusively from the Pt surface, leaving the $Fe_3O_4$ surface unreacted (Figure 19c). This general result can be likened to regiospecificity in molecular systems, because it resulted in a particular M-Pt-$Fe_3O_4$ connectivity.

A series of control experiments was designed to probe the chemoselectivity of seeded growth for a prototype heterotrimer system, Ag-Pt-$Fe_3O_4$, by using the knowledge that Ag adds to either Pt or $Fe_3O_4$ seeds under identical reaction conditions (Figure 19e–h).[190] When a physical mixture of $Fe_3O_4$ and Pt seeds was used, both Ag-$Fe_3O_4$ and Ag-Pt

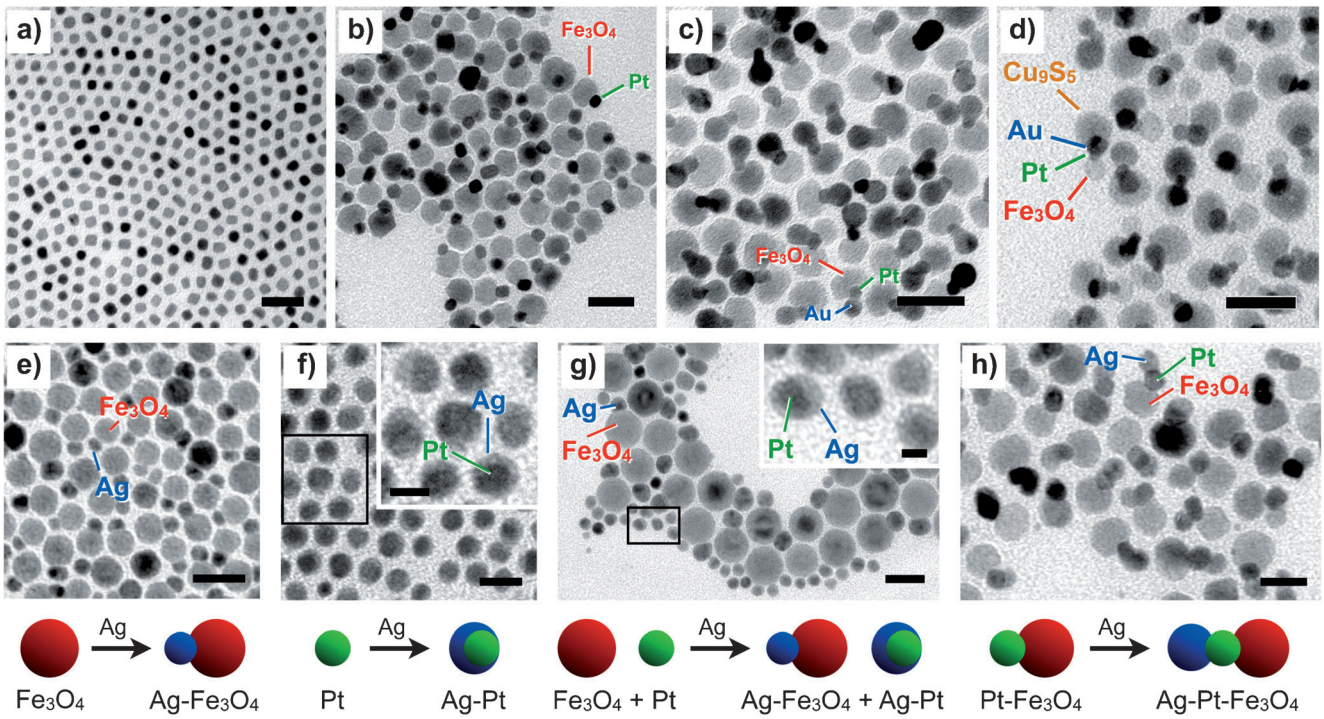


***Figure 19.*** a–d) TEM images showing the stepwise construction of linear nanoparticle heterotetramers: a) Pt nanoparticles, b) Pt-$Fe_3O_4$ heterodimers, c) Au-Pt-$Fe_3O_4$ heterotrimers, and d) $Cu_9S_5$-Au-Pt-$Fe_3O_4$ heterotetramers. e–h) TEM images and schematic representations showing a series of control experiments (same synthetic conditions for all steps) aimed at understanding the site-selective deposition of Ag onto Pt-$Fe_3O_4$ heterodimers: e) Ag grown off $Fe_3O_4$ nanoparticles, f) Ag grown off Pt nanoparticles, g) Ag grown indiscriminately off both $Fe_3O_4$ and Pt nanoparticles when both are present as a physical mixture, and h) Ag grown exclusively off the Pt domain when Pt and $Fe_3O_4$ are directly attached as heterodimers. Reprinted from Ref. [174] with permission (Copyright 2011, Macmillan Publishers Limited).

heterodimers were generated in the same reaction, with no chemoselectivity: Ag did not show a preference for growth from either $Fe_3O_4$ or Pt (Figure 19g). Under identical conditions, however, Ag grew exclusively from the Pt surface when Pt-$Fe_3O_4$ heterodimers were used, with no evidence of Ag growth from the $Fe_3O_4$ domains (Figure 19h). This clearly indicates that the hybrid particles with adjoined Pt and $Fe_3O_4$ domains have significantly different reactivity toward the seeded growth of Ag than when the Pt and $Fe_3O_4$ domains are separated. X-ray photoelectron spectroscopy (XPS) measurements showed a shift toward lower binding energies (ca. 0.5 eV) for Pt 4f electrons in the Pt-$Fe_3O_4$ heterodimers, compared to in the Pt seeds. This suggests that the Pt domain acquired a higher negative charge when connected to $Fe_3O_4$, which is attributed to electron transfer from $Fe_3O_4$. The modified Pt domain was expected to exhibit enhanced polarizability and "softness", which may have attracted the metal cations, or aided in their reduction, ultimately increasing the likelihood that heterogeneous nucleation occurred at the Pt surface. It is interesting to consider this observation as a nanoparticle analogue of a molecular substituent effect, because the presence of $Fe_3O_4$ exerts a powerful influence over the reactivity of the Pt domain through a putative electron-donation process.

Following site-selective addition of Au domains to Pt-$Fe_3O_4$ seeds, an additional seeded-growth reaction generated the first known examples of heterotetramers: colloidal hybrid nanoparticles with four distinct functional components (Figure 19d). The growth of copper sulfide ($Cu_9S_5$) domains from Au-Pt-$Fe_3O_4$ seeds was also site selective, and resulted exclusively in linear heterotetramers with $Cu_9S_5$-Au-Pt-$Fe_3O_4$ connectivity, where $Cu_9S_5$ grew only from the Au surface (Figure 19d). Replacing the copper precursor with lead complexes generated analogous PbS-Au-Pt-$Fe_3O_4$ hybrid particles. To investigate the underlying mechanism, Au and Pt-$Fe_3O_4$ subunits of the Au-Pt-$Fe_3O_4$ seeds were soaked separately in the growth solution. After thorough washing/centrifugation cycles of the subunits, significant quantities of sulfur were found in both samples, thus indicating that sulfur adsorbs to the heterotrimer seeds without preference for the Au or Pt-$Fe_3O_4$ moieties. In control reactions, however, $Cu_9S_5$ domains grew readily from Au seeds, but did not grow from Pt-$Fe_3O_4$ heterodimers, instead resulting in a mixture of separated $Cu_9S_5$ and Pt-$Fe_3O_4$. We proposed that site-specific addition of $Cu_9S_5$ to Au-Pt-$Fe_3O_4$ heterotrimers was likely the result of the kinetically favorable adsorption of sulfur atoms onto the Au surfaces, followed by reaction with $Cu^+$, which is consistent with the hypothesis given by Prasad and co-workers for the formation of Au-PbS heterodimers.[159]

## 6. Purification, Separation, and Yield

The possibilities for designing and synthesizing complex multicomponent nanostructures are rapidly expanding, and the conceptual links between the synthesis and properties of

  

molecular and nanoscale systems are clear. As complex molecules are constructed through multistep pathways, even sequential reactions that can be carried out in high yields significantly decrease the overall yield of the final product. Consider the well-established solid-phase synthesis of polypeptides,[191] which has been optimized to occur in extremely high yield. When constructing a polypeptide that contains 26 amino acids, the final yield would be 77% if each individual amino acid coupling step could be carried out with a yield of 99%. If the yield of each step were decreased to 95%, then the overall yield of the peptide would be dramatically decreased to 25%.[192] This underscores two important issues: 1) the larger the number of reactions or steps that are required to synthesize a target product, the larger the number of possible by-products and the lower the yield of the desired product, and 2) separation of the target product from the by-products is absolutely critical for generating pure samples. This is true for both molecules and nanostructures.

The separation and purification of molecules is both routine and required, as is the reporting of product yields. The approaches to do this are also well-established and readily available to most chemists. The picture can be quite different for nanoscale systems. Most researchers perform work-up procedures and rudimentary purification procedures that separate particles from soluble by-products, excess ligands, and unreacted precursors, as well as from other particles that differ significantly in size. Simple precipitation and centrifugation procedures help with this, and placing a strong magnet next to a reaction vial can help to separate particles that are magnetic at room temperature from those that are not. However, it is more difficult and less routine to carry out separations that are capable of discriminating between particles with subtle differences, such as size (in a nominally uniform sample with some polydispersity), shape, or composition, as well as nuclearity and spatial arrangement for multicomponent nanostructures. Validating that such purification techniques are successful is also a challenge.

Existing techniques for the separation and purification of molecules—including membrane filtration, size-exclusion chromatography, solvent extraction, density gradient centrifugation, and electrophoresis—can be adapted to nanoscale systems,[82] although with some important limitations. Density gradient centrifugation has proven effective for separating particles of different sizes, shapes, materials, and polymorphs.[193–196] For hybrid particles that contain multiple inorganic domains, density gradient centrifugation has also permitted the separation of aggregates with different numbers of constituent particles, for example, monomers, dimers, trimers, tetramers, and higher-order oligomers (Figure 20).[83,197] Differential magnetic catch and release (DMCR), a liquid-phase capillary chromatography technique that separates magnetic particles on the basis of differences in their magnetic moments,[80,81] has been successful for separating mixtures of colloidal hybrid nanoparticles into their constituent fractions.[84] For example, DMCR was used to identify two distinct sizes of $Fe_3O_4$ nanoparticles that form along with colloidal hybrid Au-$Fe_3O_4$ particles, ultimately separating them and producing a sample with a significantly higher yield of the target Au-$Fe_3O_4$ particles (Figure 21).

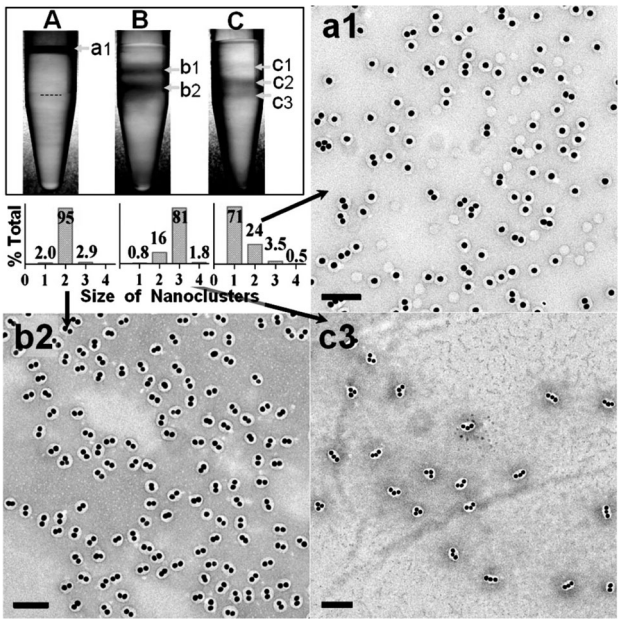


***Figure 20.*** Photograph of centrifuge tubes containing solvents layered to produce a density gradient, and TEM images and nanocluster size distributions corresponding to the fractions indicated. (Scale bar: 100 nm). Reprinted from Ref. [83] with permission (Copyright 2009, American Chemical Society).

DMCR was also used to separate two distinct populations of FePt-$Fe_3O_4$ heterodimers that appeared to be statistically identical by TEM, but that had different magnetic properties arising from subtle variations in the Fe content of the FePt domains.[84] Such separation tools will be critical both for generating pure samples of multicomponent products for which many competing by-products are possible, as well as for interrogating the physical properties inherent to a single population of particles rather than an ensemble mixture.

## 7. Summary and Outlook

Applications and fundamental scientific studies that require high-quality multifunctional nanostructures continue to expand, and they demand rigorous control over the placement and connectivity of nanoscale components in a manner that facilitates synergistic interactions. Such multicomponent systems also require robust, powerful, and highly sophisticated synthetic tools. The "total synthesis" concept used to construct complex molecules is a source of inspiration for multicomponent nanostructures because of the analogies between molecules and hybrid nanoparticles, the expanding possibilities for predictable nanoscale synthesis and modification, and the demonstration of nanoscale analogues of concepts that underpin the multistep synthesis of complex molecules. The synthesis of "artificial atoms"—high-quality nanoparticles with controllable sizes, shapes, and compositions—is becoming more mature, and a large library of available nanoparticle "synthons" is available. Nanoparticles can undergo facile chemical transformations into derivative materials with morphological retention, and this is leading to

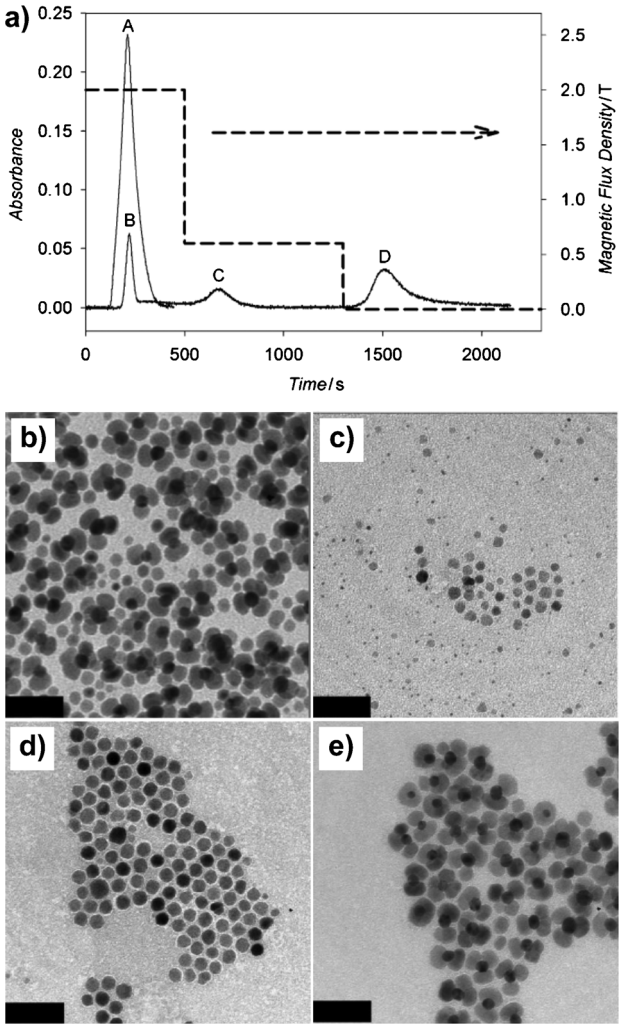


***Figure 21.*** a) Typical DMCR chromatogram showing the applied magnetic flux density (dashed line) and the absorbance, where peaks correspond to fractions that are eluted. Peak A and panel (b) correspond to the absorbance and TEM image, respectively, for as-synthesized Au-$Fe_3O_4$ heterodimers eluted with no applied magnetic field. Peaks B, C, and D correspond to the peaks eluted at the applied magnetic flux densities indicated, and the TEM images of each fraction are shown in panels (c), (d), and (e), respectively. Reprinted from Ref. [84] with permission (Copyright 2011, Wiley-VCH).

a rapidly expanding reaction library for nanoparticles that has analogies to the large and diverse library of reactions available to organic chemists. Concepts that underpin the construction of large molecules—chemoselective and regiospecific reactions, orthogonal reactivity, substituent effects, protection/deprotection strategies—are starting to be demonstrated for multicomponent nanostructures, thus adding new predictive synthesis capabilities and powerful guidelines for implementing multistep routes to complex nanostructures. When integrated, a "total synthesis" concept for hybrid nanostructures emerges, where complex multidomain nanostructures with precisely defined linkages can be constructed in a stepwise manner by sequential application of the available nanoparticle transformation reactions. Finally, methods are emerging for the separation of target products from undesired by-products. Such purification strategies are important because of the decreasing product yield that is inherent as the number of synthetic steps increases.

While a "total synthesis" approach to the construction of multicomponent nanostructures is clearly feasible and the necessary approaches are emerging, many challenges and opportunities remain. Advances in the synthesis of high-quality nanoparticles, including a deep understanding of how size and shape can be rigorously controlled, will have a direct impact on multicomponent nanostructures, since the quality of the nanoparticle synthons directly defines the upper limit of quality that can be achieved for the hybrid nanostructures from which they are constructed. An expanded nanoparticle reaction library is urgently needed, with new classes of chemical transformation reactions, greater generality across a larger range of materials, and a deeper understanding of how they can be carried out with maximum morphological retention. Preliminary demonstrations of orthogonal reactivity and protection/deprotection strategies, along with increasingly sophisticated examples of site-selective reactivity, are promising developments, but they need to be significantly expanded, both in terms of materials diversity and mechanistic understanding. Much remains to be learned about the integration and stepwise application of multiple nanoparticle reactions into multistep sequences: the identification of cross-reactivity and competitive reactions, maintaining interfacial stability, minimizing undesired by-products, and producing the highest-quality target products in a high-yielding manner. Aproaches are already in place for constructing new multicomponent nanostructures with sophisticated architectures and applications in diverse areas such as energy conversion and medicine. However, as researchers continue to advance the scientific tools that underpin a "total synthesis" concept for multicomponent nanostructures, additional applications will emerge, and possibilities for by-design synthesis will become much more sophisticated, diverse, and mainstream.

*We thank the U.S. National Science Foundation, grants CHE-0845258 and CHE-1213475, for financial support.*

Received: September 7, 2012
Published online: April 22, 2013

[1] N. Tian, Z.-Y. Zhou, S.-G. Sun, Y. Ding, Z. L. Wang, *Science* **2007**, *316*, 732.
[2] T. Yu, D. Y. Kim, H. Zhang, Y. Xia, *Angew. Chem.* **2011**, *123*, 2825; *Angew. Chem. Int. Ed.* **2011**, *50*, 2773.
[3] X. Huang, Z. Zhao, J. Fan, Y. Tan, N. Zheng, *J. Am. Chem. Soc.* **2011**, *133*, 4718.
[4] M. Jin, H. Zhang, Z. Xie, Y. Xia, *Angew. Chem.* **2011**, *123*, 7996; *Angew. Chem. Int. Ed.* **2011**, *50*, 7850.
[5] N. Tian, Z.-Y. Zhou, N.-F. Yu, L.-Y. Wang, S.-G. Sun, *J. Am. Chem. Soc.* **2010**, *132*, 7580.
[6] J. Zhang, M. R. Langille, M. L. Personick, K. Zhang, S. Li, C. A. Mirkin, *J. Am. Chem. Soc.* **2010**, *132*, 14012.
[7] L. Zhang, J. Zhang, Q. Kuang, S. Xie, Z. Jiang, Z. Xie, L. Zheng, *J. Am. Chem. Soc.* **2011**, *133*, 17114.
[8] Y.-J. Deng, N. Tian, Z.-Y. Zhou, R. Huang, Z.-L. Liu, J. Xiao, S.-G. Sun, *Chem. Sci.* **2012**, *3*, 1157.

  

[9] X. Han, M. Jin, S. Xie, Q. Kuang, Z. Jiang, Y. Jiang, Z. Xie, L. Zheng, *Angew. Chem.* **2009**, *121*, 9344; *Angew. Chem. Int. Ed.* **2009**, *48*, 9180.
[10] H. G. Yang, C. H. Sun, S. Z. Qiao, J. Zou, G. Liu, S. C. Smith, H. M. Cheng, G. Q. Lu, *Nature* **2008**, *453*, 638.
[11] H. G. Yang, G. Liu, S. Z. Qiao, C. H. Sun, Y. G. Jin, S. C. Smith, J. Zou, H. M. Cheng, G. Q. Lu, *J. Am. Chem. Soc.* **2009**, *131*, 4078.
[12] W.-C. Huang, L.-M. Lyu, Y.-C. Yang, M. H. Huang, *J. Am. Chem. Soc.* **2012**, *134*, 1261.
[13] B. Lang, R. W. Joyner, G. A. Somorjai, *Surf. Sci.* **1972**, *30*, 454.
[14] M. A. Van Hove, G. A. Somorjai, *Surf. Sci.* **1980**, *92*, 489.
[15] Z. Quan, Y. Wang, J. Fang, *Acc. Chem. Res.* **2012**, *46*, 191.
[16] M. H. Huang, P.-H. Lin, *Adv. Funct. Mater.* **2012**, *22*, 14.
[17] Z.-Y. Zhou, N. Tian, J.-T. Li, I. Broadwell, S.-G. Sun, *Chem. Soc. Rev.* **2011**, *40*, 4167.
[18] J.-H. Lee, Y.-M. Huh, Y. Jun, J. Seo, J. Jang, H.-T. Song, S. Kim, E.-J. Cho, H.-G. Yoon, J.-S. Suh, J. Cheon, *Nat. Med.* **2007**, *13*, 95.
[19] D. Ho, X. Sun, S. Sun, *Acc. Chem. Res.* **2011**, *44*, 875.
[20] J. Xie, G. Liu, H. S. Eden, H. Ai, X. Chen, *Acc. Chem. Res.* **2011**, *44*, 883.
[21] F. X. Redl, K.-S. Cho, C. B. Murray, S. O'Brien, *Nature* **2003**, *423*, 968.
[22] Z. Chen, S. O'Brien, *ACS Nano* **2008**, *2*, 1219.
[23] M. I. Bodnarchuk, M. V. Kovalenko, W. Heiss, D. V. Talapin, *J. Am. Chem. Soc.* **2010**, *132*, 11967.
[24] J. Henzie, M. Grunwald, A. Widmer-Cooper, P. L. Geissler, P. Yang, *Nat. Mater.* **2012**, *11*, 131.
[25] D. V. Talapin, J.-S. Lee, M. V. Kovalenko, E. V. Shevchenko, *Chem. Rev.* **2010**, *110*, 389.
[26] L. Carbone, P. D. Cozzoli, *Nano Today* **2010**, *5*, 449.
[27] R. Costi, A. E. Saunders, U. Banin, *Angew. Chem.* **2010**, *122*, 4996; *Angew. Chem. Int. Ed.* **2010**, *49*, 4878.
[28] P. D. Cozzoli, T. Pellegrino, L. Manna, *Chem. Soc. Rev.* **2006**, *35*, 1195.
[29] C. Wang, C. Xu, H. Zeng, S. Sun, *Adv. Mater.* **2009**, *21*, 3045.
[30] M. Casavola, R. Buonsanti, G. Caputo, P. D. Cozzoli, *Eur. J. Inorg. Chem.* **2008**, 837.
[31] A. J. Mieszawska, R. Jalilian, G. U. Sumanasekera, F. P. Zamborini, *Small* **2007**, *3*, 722.
[32] J. Hu, Y. Bando, D. Golberg, *J. Mater. Chem.* **2009**, *19*, 330.
[33] X. Feng, G. Hu, J. Hu, *Nanoscale* **2011**, *3*, 2099.
[34] R. G. Chaudhuri, S. Paria, *Chem. Rev.* **2012**, *112*, 2373.
[35] R. Agarwal, *Small* **2008**, *4*, 1872.
[36] M. Haruta, S. Tsubota, T. Kobayashi, H. Kageyama, M. J. Genet, B. Delmon, *J. Catal.* **1993**, *144*, 175.
[37] M. Haruta, *Catal. Today* **1997**, *36*, 153.
[38] M. G. Walter, E. L. Warren, J. R. McKone, S. W. Boettcher, Q. X. Mi, E. A. Santori, N. S. Lewis, *Chem. Rev.* **2010**, *110*, 6446.
[39] I. Mora-Seró, J. Bisquert, *J. Phys. Chem. Lett.* **2010**, *1*, 3046.
[40] S. Y. Reece, J. A. Hamel, K. Sung, T. D. Jarvi, A. J. Esswein, J. J. H. Pijpers, D. G. Nocera, *Science* **2011**, *334*, 645.
[41] K. Maeda, K. Domen, *J. Phys. Chem. Lett.* **2010**, *1*, 2655.
[42] P. V. Kamat, *J. Phys. Chem. Lett.* **2012**, *3*, 663.
[43] G. I. Koleilat, X. Wang, E. H. Sargent, *Nano Lett.* **2012**, *12*, 3043.
[44] J. Gao, C. L. Perkins, J. M. Luther, M. C. Hanna, H.-Y. Chen, O. E. Semonin, A. J. Nozik, R. J. Ellingson, M. C. Beard, *Nano Lett.* **2011**, *11*, 3263.
[45] B. H. Meekins, P. V. Kamat, *J. Phys. Chem. Lett.* **2011**, *2*, 2304.
[46] C. L. Choi, A. P. Alivisatos, *Annu. Rev. Phys. Chem.* **2010**, *61*, 369.
[47] E. Duguet, A. Desert, A. Perro, S. Ravaine, *Chem. Soc. Rev.* **2011**, *40*, 941.
[48] R. Costi, A. E. Saunders, E. Elmalem, A. Salant, U. Banin, *Nano Lett.* **2008**, *8*, 637.
[49] R. Costi, G. Cohen, A. Salant, E. Rabani, U. Banin, *Nano Lett.* **2009**, *9*, 2031.
[50] S. Kumar, M. Jones, S. S. Lo, G. D. Scholes, *Small* **2007**, *3*, 1633.
[51] S. Kim, B. Fisher, H. J. Eisler, M. Bawendi, *J. Am. Chem. Soc.* **2003**, *125*, 11466.
[52] C. Galland, Y. Ghosh, A. Steinbruck, M. Sykora, J. A. Hollingsworth, V. I. Klimov, H. Htoon, *Nature* **2011**, *479*, 203.
[53] C. Galland, Y. Ghosh, A. Steinbruck, J. A. Hollingsworth, H. Htoon, V. I. Klimov, *Nat. Commun.* **2012**, *3*, 908.
[54] L. Amirav, A. P. Alivisatos, *J. Phys. Chem. Lett.* **2010**, *1*, 1051.
[55] K. P. Acharya, R. S. Khnayzer, T. O'Connor, G. Diederich, M. Kirsanova, A. Klinkova, D. Roth, E. Kinder, M. Imboden, M. Zamkov, *Nano Lett.* **2011**, *11*, 2919.
[56] P. Li, Z. Wei, T. Wu, Q. Peng, Y. Li, *J. Am. Chem. Soc.* **2011**, *133*, 5660.
[57] H. Yin, C. Wang, H. G. Zhu, S. H. Overbury, S. Sun, S. Dai, *Chem. Commun.* **2008**, 4357.
[58] C. Wang, H. Daimon, S. Sun, *Nano Lett.* **2009**, *9*, 1493.
[59] C. Wang, H. Yin, S. Dai, S. Sun, *Chem. Mater.* **2010**, *22*, 3277.
[60] A. Figuerola, A. Fiore, R. Di Corato, A. Falqui, C. Giannini, E. Micotti, A. Lascialfari, M. Corti, R. Cingolani, T. Pellegrino, P. D. Cozzoli, L. Manna, *J. Am. Chem. Soc.* **2008**, *130*, 1477.
[61] M. I. Bodnarchuk, M. V. Kovalenko, H. Groiss, R. Resel, M. Reissner, G. Hesser, R. T. Lechner, W. Steiner, F. Schaffler, W. Heiss, *Small* **2009**, *5*, 2247.
[62] S. Deka, A. Falqui, G. Bertoni, C. Sangregorio, G. Poneti, G. Morello, M. De Giorgi, C. Giannini, R. Cingolani, L. Manna, P. D. Cozzoli, *J. Am. Chem. Soc.* **2009**, *131*, 12817.
[63] C. D. Keating, M. J. Natan, *Adv. Mater.* **2003**, *15*, 451.
[64] T. R. Kline, M. Tian, J. Wang, A. Sen, M. W. H. Chan, T. E. Mallouk, *Inorg. Chem.* **2006**, *45*, 7555.
[65] W. F. Paxton, K. C. Kistler, C. C. Olmeda, A. Sen, S. K. St Angelo, Y. Cao, T. E. Mallouk, P. E. Lammert, V. H. Crespi, *J. Am. Chem. Soc.* **2004**, *126*, 13424.
[66] T. R. Kline, W. F. Paxton, T. E. Mallouk, A. Sen, *Angew. Chem.* **2005**, *117*, 754; *Angew. Chem. Int. Ed.* **2005**, *44*, 744.
[67] W. Wang, L. A. Castro, M. Hoyos, T. E. Mallouk, *ACS Nano* **2012**, *6*, 6122.
[68] A. K. Salem, J. Chao, K. W. Leong, P. C. Searson, *Adv. Mater.* **2004**, *16*, 268.
[69] J. C. Love, A. R. Urbach, M. G. Prentiss, G. M. Whitesides, *J. Am. Chem. Soc.* **2003**, *125*, 12696.
[70] B. D. Smith, D. J. Kirby, C. D. Keating, *Small* **2011**, *7*, 781.
[71] D. J. Peña, J. K. N. Mbindyo, A. J. Carado, T. E. Mallouk, C. D. Keating, B. Razavi, T. S. Mayer, *J. Phys. Chem. B* **2002**, *106*, 7458.
[72] S. R. Nicewarner-Pena, R. G. Freeman, B. D. Reiss, L. He, D. J. Pena, I. D. Walton, R. Cromer, C. D. Keating, M. J. Natan, *Science* **2001**, *294*, 137.
[73] S. E. Brunker, K. B. Cederquist, C. D. Keating, *Nanomedicine* **2007**, *2*, 695.
[74] R. L. Stoermer, K. B. Cederquist, S. K. McFarland, M. Y. Sha, S. G. Penn, C. D. Keating, *J. Am. Chem. Soc.* **2006**, *128*, 16892.
[75] F. Liu, J. Y. Lee, W. Zhou, *J. Phys. Chem. B* **2004**, *108*, 17959.
[76] F. Liu, J. Y. Lee, W. Zhou, *Adv. Funct. Mater.* **2005**, *15*, 1459.
[77] F. Liu, J. Y. Lee, W. Zhou, *Small* **2006**, *2*, 121.
[78] M. Casavola, V. Grillo, E. Carlino, C. Giannini, F. Gozzo, E. F. Pinel, M. A. Garcia, L. Manna, R. Cingolani, P. D. Cozzoli, *Nano Lett.* **2007**, *7*, 1386.
[79] R. Buonsanti, V. Grillo, E. Carlino, C. Giannini, F. Gozzo, M. Garcia-Hernandez, M. A. Garcia, R. Cingolani, P. D. Cozzoli, *J. Am. Chem. Soc.* **2010**, *132*, 2437.
[80] A. H. Latham, R. S. Freitas, P. Schiffer, M. E. Williams, *Anal. Chem.* **2005**, *77*, 5055.
[81] J. S. Beveridge, J. R. Stephens, A. H. Latham, M. E. Williams, *Anal. Chem.* **2009**, *81*, 9618.

  

[82] B. Kowalczyk, I. Lagzi, B. A. Grzybowski, *Curr. Opin. Colloid Interface Sci.* **2011**, *16*, 135 – 148.
[83] G. Chen, Y. Wang, L. H. Tan, M. Yang, L. S. Tan, Y. Chen, H. Chen, *J. Am. Chem. Soc.* **2009**, *131*, 4218.
[84] J. S. Beveridge, M. R. Buck, J. F. Bondi, R. Misra, P. Schiffer, R. E. Schaak, M. E. Williams, *Angew. Chem. Int. Ed.* **2011**, *50*, 9875.
[85] K. C. Nicolaou, D. Vourloumis, N. Winssinger, P. S. Baran, *Angew. Chem.* **2000**, *112*, 46; *Angew. Chem. Int. Ed.* **2000**, *39*, 44.
[86] W. A. Smit, A. F. Bochkov, R. Caple, *Organic Synthesis*: *The Science Behind the Art*, Royal Society of Chemistry, Cambridge, **1998**.
[87] K. C. Nicolaou, C. R. H. Hale, C. Nilewski, H. A. Ioannidou, *Chem. Soc. Rev.* **2012**, *41*, 5185.
[88] E. J. Corey, X.-M. Cheng, *The Logic of Chemical Synthesis*, Wiley, New York, **1989**.
[89] E. J. Corey, *Chem. Soc. Rev.* **1988**, *17*, 111.
[90] S. D. Roughley, A. M. Jordan, *Med. Chem.* **2011**, *54*, 3451.
[91] B. M. Trost, *Science* **1983**, *219*, 245.
[92] R. A. Shenvi, D. P. O'Malley, P. S. Baran, *Acc. Chem. Res.* **2009**, *42*, 530.
[93] N. A. Afagh, A. K. Yudin, *Angew. Chem.* **2010**, *122*, 270; *Angew. Chem. Int. Ed.* **2010**, *49*, 262.
[94] P. G. M. Wuts, T. W. Greene, T. W. Greene, *Greene's Protective Groups in Organic Synthesis*, 4th ed., Wiley-Interscience, Hoboken, **2007**.
[95] B. M. Trost, *Science* **1991**, *254*, 1471.
[96] T. Newhouse, P. S. Baran, R. W. Hoffmann, *Chem. Soc. Rev.* **2009**, *38*, 3010.
[97] T. Gaich, P. S. Baran, *J. Org. Chem.* **2010**, *75*, 4657.
[98] D. V. Talapin, Y. Yin, *J. Mater. Chem.* **2011**, *21*, 11454.
[99] Y. Vasquez, A. E. Henkes, J. C. Bauer, R. E. Schaak, *J. Solid State Chem.* **2008**, *181*, 1509.
[100] G. D. Moon, S. Ko, Y. Min, J. Zeng, Y. Xia, U. Jeong, *Nano Today* **2011**, *6*, 186.
[101] Y. Yin, R. M. Rioux, C. K. Erdonmez, S. Hughes, G. A. Somorjai, A. P. Alivisatos, *Science* **2004**, *304*, 711.
[102] Y. Yin, C. K. Erdonmez, A. Cabot, S. Hughes, A. P. Alivisatos, *Adv. Funct. Mater.* **2006**, *16*, 1389.
[103] A. E. Henkes, R. E. Schaak, *Chem. Mater.* **2007**, *19*, 4234.
[104] H. Zhang, D.-H. Ha, R. Hovden, L. F. Kourkoutis, R. D. Robinson, *Nano Lett.* **2011**, *11*, 188.
[105] R. E. Schaak, A. K. Sra, B. M. Leonard, R. E. Cable, J. C. Bauer, Y. F. Han, J. Means, W. Teizer, Y. Vasquez, E. S. Funck, *J. Am. Chem. Soc.* **2005**, *127*, 3506.
[106] J. C. Bauer, X. Chen, Q. Liu, T.-H. Phan, R. E. Schaak, *J. Mater. Chem.* **2008**, *18*, 275.
[107] B. M. Leonard, M. E. Anderson, K. D. Oyler, T.-H. Phan, R. E. Schaak, *ACS Nano* **2009**, *3*, 940.
[108] F. Pinna, *Catal. Today* **1998**, *41*, 129.
[109] I. T. Sines, R. E. Schaak, *J. Am. Chem. Soc.* **2011**, *133*, 1294.
[110] D. H. Son, S. M. Hughes, Y. Yin, A. P. Alivisatos, *Science* **2004**, *306*, 1009.
[111] P. H. C. Camargo, Y. H. Lee, U. Jeong, Z. Q. Zou, Y. Xia, *Langmuir* **2007**, *23*, 2985.
[112] R. D. Robinson, B. Sadtler, D. O. Demchenko, C. K. Erdonmez, L.-W. Wang, A. P. Alivisatos, *Science* **2007**, *317*, 355.
[113] S. E. Wark, C.-H. Hsia, D. H. Son, *J. Am. Chem. Soc.* **2008**, *130*, 9550.
[114] J. M. Luther, H. Zheng, B. Sadtler, A. P. Alivisatos, *J. Am. Chem. Soc.* **2009**, *131*, 16851.
[115] B. Sadtler, D. O. Demchenko, H. Zheng, S. M. Hughes, M. G. Merkle, U. Dahmen, L.-W. Wang, A. P. Alivisatos, *J. Am. Chem. Soc.* **2009**, *131*, 5285.
[116] P. K. Jain, L. Amirav, S. Aloni, A. P. Alivisatos, *J. Am. Chem. Soc.* **2010**, *132*, 9997.
[117] H. Li, M. Zanella, A. Genovese, M. Povia, A. Falqui, C. Giannini, L. Manna, *Nano Lett.* **2011**, *11*, 4964.
[118] M. Casavola, M. A. van Huis, S. Bals, K. Lambert, Z. Hens, D. Vanmaekelbergh, *Chem. Mater.* **2012**, *24*, 294.
[119] H. Li, R. Brescia, R. Krahne, G. Bertoni, M. J. P. Alcocer, C. D'Andrea, F. Scotognella, F. Tassone, M. Zanella, M. De Giorgi, L. Manna, *ACS Nano* **2012**, *6*, 1637.
[120] F. Dawood, R. E. Schaak, *J. Am. Chem. Soc.* **2009**, *131*, 424.
[121] J. Park, H. Zheng, Y.-W. Jun, A. P. Alivisatos, *J. Am. Chem. Soc.* **2009**, *131*, 13943.
[122] M. Saruyama, Y.-G. So, K. Kimoto, S. Taguchi, Y. Kanemitsu, T. Teranishi, *J. Am. Chem. Soc.* **2011**, *133*, 17598.
[123] Y. Wei, R. Klajn, A. O. Pinchuk, B. A. Grzybowski, *Small* **2008**, *4*, 1635.
[124] H. Wu, O. Chen, J. Zhuang, J. Lynch, D. LaMontagne, Y. Nagaoka, Y. C. Cao, *J. Am. Chem. Soc.* **2011**, *133*, 14327.
[125] G. Krylova, L. J. Giovanetti, F. G. Requejo, N. M. Dimitrijevic, A. Prakapenka, E. V. Shevchenko, *J. Am. Chem. Soc.* **2012**, *134*, 4384.
[126] Y. Xia, Y. Xiong, B. Lim, S. E. Skrabalak, *Angew. Chem.* **2009**, *121*, 62; *Angew. Chem. Int. Ed.* **2009**, *48*, 60.
[127] C. M. Cobley, M. Rycenga, F. Zhou, Z.-Y. Li, Y. Xia, *Angew. Chem.* **2009**, *121*, 4918; *Angew. Chem. Int. Ed.* **2009**, *48*, 4824.
[128] M. J. Mulvihill, X. Y. Ling, J. Henzie, P. Yang, *J. Am. Chem. Soc.* **2010**, *132*, 268.
[129] B. Lim, Y. Xia, *Angew. Chem.* **2011**, *123*, 78; *Angew. Chem. Int. Ed.* **2011**, *50*, 76.
[130] Y. Sun, Y. Xia, *J. Am. Chem. Soc.* **2004**, *126*, 3892.
[131] X. Lu, H.-Y. Tuan, J. Chen, Z.-Y. Li, B. A. Korgel, Y. N. Xia, *J. Am. Chem. Soc.* **2007**, *129*, 1733.
[132] S. E. Skrabalak, L. Au, X. D. Li, Y. N. Xia, *Nat. Protoc.* **2007**, *2*, 2182.
[133] H. Zhang, M. Jin, J. Wang, W. Li, P. H. C. Camargo, M. Kim, D. Yang, Z. Xie, Y. Xia, *J. Am. Chem. Soc.* **2011**, *133*, 6078.
[134] N. J. Halas, S. Lal, W.-S. Chang, S. Link, P. Nordlander, *Chem. Rev.* **2011**, *111*, 3913.
[135] M. Niederberger, H. Colfen, *Phys. Chem. Chem. Phys.* **2006**, *8*, 3271.
[136] D. Seo, C. Il Yoo, J. Jung, H. Song, *J. Am. Chem. Soc.* **2008**, *130*, 2940.
[137] E. V. Shevchenko, M. I. Bodnarchuk, M. V. Kovalenko, D. V. Talapin, R. K. Smith, S. Aloni, W. Heiss, A. P. Alivisatos, *Adv. Mater.* **2008**, *20*, 4323.
[138] J. Gao, G. Liang, J. S. Cheung, Y. Pan, Y. Kuang, F. Zhao, B. Zhang, X. Zhang, E. X. Wu, B. Xu, *J. Am. Chem. Soc.* **2008**, *130*, 11828.
[139] J. Gao, G. Liang, B. Zhang, Y. Kuang, X. Zhang, B. Xu, *J. Am. Chem. Soc.* **2007**, *129*, 1428.
[140] G. Zhang, H. Fang, H. Yang, L. A. Jauregui, Y. P. Chen, Y. Wu, *Nano Lett.* **2012**, *12*, 3627.
[141] L. Manna, E. C. Scher, A. P. Alivisatos, *J. Am. Chem. Soc.* **2000**, *122*, 12700.
[142] Z. A. Peng, X. Peng, *J. Am. Chem. Soc.* **2001**, *123*, 1389.
[143] T. Mokari, E. Rothenberg, I. Popov, R. Costi, U. Banin, *Science* **2004**, *304*, 1787.
[144] S. Kudera, L. Carbone, M. F. Casula, R. Cingolani, A. Falqui, E. Snoeck, W. J. Parak, L. Manna, *Nano Lett.* **2005**, *5*, 445.
[145] L. Carbone et al., *Nano Lett.* **2007**, *7*, 2942.
[146] G. Dukovic, M. G. Merkle, J. H. Nelson, S. M. Hughes, A. P. Alivisatos, *Adv. Mater.* **2008**, *20*, 4306.
[147] G. Menagen, D. Mocatta, A. Salant, I. Popov, D. Dorfs, U. Banin, *Chem. Mater.* **2008**, *20*, 6900.
[148] L. Carbone, A. Jakab, Y. Khalavka, C. Sonnichsen, *Nano Lett.* **2009**, *9*, 3710.
[149] X. Li, J. Lian, M. Lin, Y. Chan, *J. Am. Chem. Soc.* **2011**, *133*, 672.

  

[150] S. Chakrabortty, J. A. Yang, Y. M. Tan, N. Mishra, Y. Chan, *Angew. Chem.* **2010**, *122*, 2950; *Angew. Chem. Int. Ed.* **2010**, *49*, 2888.
[151] X. Chen, Y. Lou, A. C. Samia, C. Burda, *Nano Lett.* **2003**, *3*, 799.
[152] A. Aharoni, T. Mokari, I. Popov, U. Banin, *J. Am. Chem. Soc.* **2006**, *128*, 257.
[153] L. Manna, E. C. Scher, L.-S. Li, A. P. Alivisatos, *J. Am. Chem. Soc.* **2002**, *124*, 7136.
[154] D. V. Talapin, I. Mekis, S. Gotzinger, A. Kornowski, O. Benson, H. Weller, *J. Phys. Chem. B* **2004**, *108*, 18826.
[155] S. Deka, A. Quarta, M. G. Lupo, A. Falqui, S. Boninelli, C. Giannini, G. Morello, M. De Giorgi, G. Lanzani, C. Spinella, R. Cingolani, T. Pellegrino, L. Manna, *J. Am. Chem. Soc.* **2009**, *131*, 2948.
[156] A. Eychmüller, A. Mews, H. Weller, *Chem. Phys. Lett.* **1993**, *208*, 59.
[157] D. Schooss, A. Mews, A. Eychmuller, H. Weller, *Phys. Rev. B* **1994**, *49*, 17072.
[158] Z. Xu, Y. Hou, S. Sun, *J. Am. Chem. Soc.* **2007**, *129*, 8698.
[159] W. Shi, H. Zeng, Y. Sahoo, T. Y. Ohulchanskyy, Y. Ding, Z. L. Wang, M. Swihart, P. N. Prasad, *Nano Lett.* **2006**, *6*, 875.
[160] W. Shi, Y. Sahoo, H. Zeng, Y. Ding, M. T. Swihart, P. N. Prasad, *Adv. Mater.* **2006**, *18*, 1889.
[161] T. Chen, G. Chen, S. Xing, T. Wu, H. Chen, *Chem. Mater.* **2010**, *22*, 3826.
[162] T. Ung, L. M. Liz-Marzan, P. Mulvaney, *Langmuir* **1998**, *14*, 3740.
[163] H.-T. Zhang, J. Ding, G.-M. Chow, Z.-L. Dong, *Langmuir* **2008**, *24*, 13197.
[164] L. Qin, S. Park, L. Huang, C. A. Mirkin, *Science* **2005**, *309*, 113.
[165] X. Chen, Y.-M. Jeon, J.-W. Jang, L. Qin, F. Huo, W. Wei, C. A. Mirkin, *J. Am. Chem. Soc.* **2008**, *130*, 8166.
[166] L. Qin, S. Zou, C. Xue, A. Atkinson, G. C. Schatz, C. A. Mirkin, *Proc. Natl. Acad. Sci. USA* **2006**, *103*, 13300.
[167] L. Qin, M. J. Banholzer, J. E. Millstone, C. A. Mirkin, *Nano Lett.* **2007**, *7*, 3849.
[168] M. McEachran, D. Keogh, B. Pietrobon, N. Cathcart, I. Gourevich, N. Coombs, V. Kitaev, *J. Am. Chem. Soc.* **2011**, *133*, 8066.
[169] X. Lu, L. Au, J. McLellan, Z.-Y. Li, M. Marquez, Y. Xia, *Nano Lett.* **2007**, *7*, 1764.
[170] X. Guo, Q. Zhang, Y. Sun, Q. Zhao, J. Yang, *ACS Nano* **2012**, *6*, 1165.
[171] Y. Lee, M. A. Garcia, N. A. F. Huls, S. Sun, *Angew. Chem.* **2010**, *122*, 1293; *Angew. Chem. Int. Ed.* **2010**, *49*, 1271.
[172] C. George, D. Dorfs, G. Bertoni, A. Falqui, A. Genovese, T. Pellegrino, A. Roig, A. Quarta, R. Comparelli, M. L. Curri, R. Cingolani, L. Manna, *J. Am. Chem. Soc.* **2011**, *133*, 2205.
[173] F. Gao, S. Mukherjee, Q. Cui, Z. Gu, *J. Phys. Chem. C* **2009**, *113*, 9546.
[174] M. R. Buck, J. F. Bondi, R. E. Schaak, *Nat. Chem.* **2012**, *4*, 37.
[175] R. Lavieville, Y. Zhang, A. Casu, A. Genovese, L. Manna, E. Di Fabrizio, R. Krahne, *ACS Nano* **2012**, *6*, 2940.
[176] A. Figuerola, I. R. Franchini, A. Fiore, R. Mastria, A. Falqui, G. Bertoni, S. Bals, G. Van Tendeloo, S. Kudera, R. Cingolani, L. Manna, *Adv. Mater.* **2009**, *21*, 550.
[177] A. Figuerola, M. van Huis, M. Zanella, A. Genovese, S. Marras, A. Falqui, H. W. Zandbergen, R. Cingolani, L. Manna, *Nano Lett.* **2010**, *10*, 3028.
[178] T. Teranishi, M. Saruyama, M. Nakaya, M. Kanehara, *Angew. Chem.* **2007**, *119*, 1743; *Angew. Chem. Int. Ed.* **2007**, *46*, 1713.
[179] M. Saruyama, M. Kanehara, T. Teranishi, *Chem. Commun.* **2009**, 2724.
[180] M. E. Anderson, M. R. Buck, I. T. Sines, K. D. Oyler, R. E. Schaak, *J. Am. Chem. Soc.* **2008**, *130*, 14042.
[181] N. R. Jana, L. Gearheart, S. O. Obare, C. J. Murphy, *Langmuir* **2002**, *18*, 922.
[182] Z. Bao, Z. Sun, M. Xiao, H. Chen, L. Tian, J. Wang, *J. Mater. Chem.* **2011**, *21*, 11537.
[183] Y. Ridelman, G. Singh, R. Popovitz-Biro, S. G. Wolf, S. Das, R. Klajn, *Small* **2012**, *8*, 654.
[184] J. K. Sahoo, M. N. Tahir, F. Hoshyargar, B. Nakhjavan, R. Branscheid, U. Kolb, W. Tremel, *Angew. Chem.* **2011**, *123*, 12479; *Angew. Chem. Int. Ed.* **2011**, *50*, 12271.
[185] N. S. Lewis, D. G. Nocera, *Proc. Natl. Acad. Sci. USA* **2007**, *104*, 20142.
[186] M. A. Hines, P. Guyot-Sionnest, *J. Phys. Chem.* **1996**, *100*, 468.
[187] X. Peng, M. C. Schlamp, A. V. Kadavanich, A. P. Alivisatos, *J. Am. Chem. Soc.* **1997**, *119*, 7019.
[188] Y. Chen, J. Vela, H. Htoon, J. L. Casson, D. J. Werder, D. A. Bussian, V. I. Klimov, J. A. Hollingsworth, *J. Am. Chem. Soc.* **2008**, *130*, 5026.
[189] J. Zhang, Y. Tang, K. Lee, M. Ouyang, *Science* **2010**, *327*, 1634.
[190] L. Zhang, Y.-H. Dou, H.-C. Gu, *J. Colloid Interface Sci.* **2006**, *297*, 660.
[191] R. B. Merrifield, *J. Am. Chem. Soc.* **1963**, *85*, 2149.
[192] A. A. Tseng, *Nanofabrication*: *Fundamentals and Applications*, World Scientific, Singapore, **2008**.
[193] D. Steinigeweg, M. Schutz, M. Salehi, S. Schlucker, *Small* **2011**, *7*, 2443.
[194] L. Bai, X. Ma, J. Liu, X. Sun, D. Zhao, D. G. Evans, *J. Am. Chem. Soc.* **2010**, *132*, 2333.
[195] P. Qiu, C. Mao, *Adv. Mater.* **2011**, *23*, 4880.
[196] X. Ma, Y. Kuang, L. Bai, Z. Chang, F. Wang, X. Sun, D. G. Evans, *ACS Nano* **2011**, *5*, 3242.
[197] X. Xu, S. Stottinger, G. Battagliarin, G. Hinze, E. Mugnaioli, C. Li, K. Mullen, T. Basche, *J. Am. Chem. Soc.* **2011**, *133*, 18062.